Journal of Controlled Release 361 (2023) 334–349

Contents lists available at ScienceDirect

Journal of Controlled Release

journal homepage: www.elsevier.com/locate/jconrel

Thermo-responsive Diels-Alder stabilized hydrogels for ocular drug delivery of a corticosteroid and an anti-VEGF fab fragment

Blessing C. Ilochonwu [a], Simone A. van der Lugt [a], Ada Annala [a], Greta Di Marco [a], Thibault Sampon [a], Juergen Siepmann [b,c], Florence Siepmann [b,c], Wim E. Hennink [a], Tina Vermonden [a,*]

[a] Department of Pharmaceutics, Utrecht Institute for Pharmaceutical Sciences, Faculty of Science, Utrecht University, PO box 80082, 3508, TB, Utrecht, the Netherlands
[b] University of Lille, College of Pharmacy, 3 Rue du Prof. Laguesse, 59006 Lille, France
[c] INSERM U 1008, Controlled Drug Delivery Systems and Biomaterials, 3 Rue du Prof. Laguesse, 59006 Lille, France

ARTICLE INFO

Keywords:
Hydrogel
FAB
Anti-VEGF
Dexamethasone
Diels-Alder
Injectability
In situ crosslinking

ABSTRACT

In the present study, a novel in situ forming thermosensitive hydrogel system was investigated as a versatile drug delivery system for ocular therapy. For this purpose, two thermosensitive ABA triblock copolymers bearing either furan or maleimide moieties were synthesized, named respectively poly(NIPAM-*co*-HEA/Furan)-PEG_{6K}-P(NIPAM-co-HEA/Furan) (PNF) and poly(NIPAM-co-HEA/Maleimide)-PEG_{6K}-P(NIPAM-co-HEA/−Maleimide) (PNM). Hydrogels were obtained upon mixing aqueous PNF and PNM solutions followed by incubation at 37 °C. The hydrogel undergoes an immediate (<1 min) sol-gel transition at 37 °C. In situ hydrogel formation at 37 °C was also observed after intravitreal injection of the formulation into an ex vivo rabbit eye. The hydrogel network formation was due to physical self-assembly of the PNIPAM blocks and a catalyst-free furan-maleimide Diels−Alder (DA) chemical crosslinking in the hydrophobic domains of the polymer network. Rheological studies demonstrated sol-gel transition at 23 °C, and DA crosslinks were formed in time within 60 min by increasing the temperature from 4 to 37 °C. When incubated at 37 °C, these hydrogels were stable for at least one year in phosphate buffer of pH 7.4. However, the gels degraded at basic pH 10 and 11 after 13 and 3 days, respectively, due to hydrolysis of ester bonds in the crosslinks of the hydrogel network. The hydrogel was loaded with an anti-VEGF antibody fragment (FAB; 48.4 kDa) or with corticosteroid dexamethasone (dex) by dissolving (FAB) or dispersing (DEX) in the hydrogel precursor solution. The FAB fragment in unmodified form was quantitatively released over 13 days after an initial burst release of 46, 45 and 28 % of the loading for the 5, 10 and 20 wt% hydrogel, respectively, due to gel dehydration during formation. The low molecular weight drug dexamethasone was almost quantitively released in 35 days. The slower release of dexamethasone compared to the FAB fragment can likely be explained by the solubilization of this hydrophobic drug in the hydrophobic domains of the gel. The thermosensitive gels showed good cytocompatibility when brought in contact with macrophage-like mural cells (RAW 264.7) and human retinal pigment epithelium-derived (ARPE-19) cells. This study demonstrates that PNF-PNM thermogel may be a suitable formulation for sustained release of bioactive agents into the eye for treating posterior segment eye diseases.

1. Introduction

Ocular vascular diseases are one of the leading causes of visual impairment worldwide [1–3]. In general, it has been shown that there is an increased number of pro-inflammatory cells and increased levels of vascular endothelial growth factor (VEGF) in the posterior segment of the diseased eye, resulting in neovascularization and vasopermeability [1,4]. The current treatment consists of administering anti-VEGF antibodies or an anti-inflammatory drug such as the corticosteroid dexamethasone (DEX), or a combination of these drug [5–9].

Despite being efficacious in controlling ocular neovascularization and inflammation, long-term intraocular drug therapy has certain drawbacks. After IV/oral administration only a fraction of the administered dose reaches the back of the eye due to physiological barriers

* Corresponding author.
E-mail address: t.vermonden@uu.nl (T. Vermonden).

https://doi.org/10.1016/j.jconrel.2023.07.052
Received 9 March 2023; Received in revised form 3 July 2023; Accepted 30 July 2023
Available online 10 August 2023

preventing drugs from reaching the retina [7,10]. To bypass ocular barriers, clinically used intraocular drug formulations (such as Lucentis®, Eylea®, Kenalog®-**40**) are administered by intravitreal bolus injection. The advantages of this administration route above others include immediate drug release, increased local therapeutic effects and reduced systemic adverse events [11]. The intravitreal half-life of dexamethasone in vitreous is only 5.5 h [12], while the intravitreal half-life of ranibizumab (an FDA approved anti-VEGF Fab fragment) is around three days. [6,13] Therefore, repeated injections are required for the treatment of chronic intraocular diseases [14,15]. Although conventional drug formulations such as eye drops and injectable liquids play an important role in ocular therapies, they are characterized by poor patient compliance and adverse side effects [16]. Hence, to overcome these drawbacks, there is a need for new delivery systems that provide local sustained release of loaded drugs to the retina after intravitreal injection. Several advanced delivery systems have been developed and investigated for this purpose, such as drug loaded surgically sutured implants, nanoparticles, liposomes, polymeric micelles, dendrimers, microneedles and hydrogels [16–18]. Several implants for the treatment of the posterior segment of the eye are on the market or studied in clinical trials [18] among which the non-biodegradable formulations Vitrasert®, Retisert® [19,20], Medidur®, Iluvien® [21] and the biodegradable ones Posurdex®, Ozurdex® [22,23] and Surodex® [24]. However, these implants all contain small molecules such as dexamethasone, ganciclovir or fluocinolone acetonide. However, only a few biotherapeutics-carrying implants are on the market. Genentech's Susvimo, previously called Port Delivery System with ranibizumab [25,26], is the first and only FDA-approved (in October 2021) protein refillable implant based on a porous titanium release control element used for the treatment of neovascular age-related macular degeneration [27]. Although these implants significantly prolong drug release in the posterior segment of the eye, the majority of these intraocular implants requires invasive administration methods to place the devices at the target site, and subsequent surgical procedures are often needed to remove these non-biodegradable implants.

Hydrogels, hydrophilic crosslinked polymers containing a large amount of water, are widely used for drug delivery, tissue engineering and cell encapsulation [28–32]. Furthermore, by a proper selection of their building blocks, hydrogels can be rendered biodegradable due to chemical and/or enzymatic hydrolysis [33–35]. There are a few hydrogel formulations approved by the FDA for ocular applications, among which Akten, a topical lidocaine hydrochloride ophthalmic gel [36,37]. Several hydrogel and other delivery technologies systems are currently being investigated for intravitreal protein delivery, as reviewed by Ilochonwu et al. [31] and Chang et al. [32]

In the past years, in situ forming hydrogels based on PEG and/or hyaluronic acid have received interest for ocular drug delivery applications [38,39]. These hydrogels showed in vitro sustained drug release and may play an important role in advancing the currently available ocular therapy as previously discussed by Ilochonwu et al. [38] Although significant progress has been made, several issues still have to be addressed: 1) fast in situ gelling of the formed hydrogels is needed as this limits polymer diffusion and dilution within the vitreous body after intravitreal injection and 2) unwanted side reactions between polymer functional groups and loaded drugs must be avoided.

Depending on the chemical composition of the polymer building blocks, hydrogels can be designed to respond to various stimuli, such as heat, pH and light [40–42]. An important and attractive class of hydrogels are the thermosensitive in situ forming systems. At ambient temperature, these formulations are low viscous aqueous polymeric solutions, and a temperature change (from room to physiological temperature), affects the hydrophobic and hydrophilic balance of the constituents of the polymer to induce a sol-gel transition of the formulation [40]. Poly(N-isopropylacrylamide) (PNIPAM) is a well-studied thermosensitive polymer which displays lower critical solution temperature (LCST) in aqueous solutions at around 32 °C and this polymer has been used as basis for preparation of thermosensitive hydrogels. This way, a liquid formulation can be injected into the vitreous with a minimally invasive method using a small gauge needle, avoiding a surgical intervention [43,44]. However, the physical crosslinking is reversible and yields gels with low mechanical properties [45]. Therefore chemical crosslinking has been investigated as a strategy for increasing the hydrogel strength and stabilizing the network structure [46,47]. For proper injectability, the physical and covalent gelation should only occur at the site of injection and for sure not in the applied needle which would result in unwanted obstruction. Furthermore, after ocular administration, the crosslinking reactions between the functional moieties should be relatively fast to avoid unwanted reactions and modifications of co-administered pharmaceuticals and drugs. In this study, the Diels-Alder (DA) reaction was used to stabilize the hydrogel network as chemical crosslinking strategy. In general, DA reaction is a [4 + 2] cycloaddition between a diene and dienophile to form a cyclohexene adduct and was first reported by Alder and Diels in 1929 [48]. In 2009, Wei et al. for the first time employed DA reactions for the preparation of a hydrogel [49]. The reaction between furan and maleimide is the most common DA reaction used for hydrogel crosslinking. However, unfavorable reactions between maleimides and amines or thiols present in e.g. proteins limit the application of this reaction pair for development of protein releasing hydrogels [50]. To overcome this drawback, in the present study, the reactive functional groups were designed to be predominantly located within the hydrophobic domains of the hydrogel polymeric network, to limit protein reactivity with the maleimide moieties as was observed in our previous study [38].

Therefore, to tackle the current challenges of 1) fast in-situ gelation and 2) prevention of side reactions between therapeutics and crosslinkable groups, we designed a novel injectable hydrogel system. This study investigates the combination of DA crosslinks with thermosensitive gelation. The thermo-responsive DA stabilized hydrogel formulation was characterized and evaluated as a potential drug delivery system for ocular therapy. The aim was to load the engineered hydrogel with dexamethasone and a Fab fragment of an anti-VEGF antibody as drugs and to investigate their gelation kinetics, degradation behavior and release profiles. Compared to previously discussed Diels- Alder hydrogels [35,38,39], the anticipated advantages of the present hydrogel system include faster in situ gelation due to thermo-responsive behavior, suitability for simultaneous delivery in one formulation both a biotherapeutic, preventing protein modification, and a small hydrophobic drug. Finally, intravitreal injection of the hydrogel on ex vivo rabbit eye explant and retinal cell cytocompatibility were investigated the injection procedure, in situ gel formation and the overall usability of this system for intraocular applications.

2. Material & methods

2.1. Materials

Chemicals were purchased from Sigma-Aldrich (Zwijndrecht, the Netherlands) and used as received unless mentioned otherwise. Dichloromethane (DCM) and tetrahydrofuran (THF) were dried on molecular sieves 24 h before use. Phosphate-buffered saline was composed as follows except mentioned otherwise: 0.13 M NaCl, 2.7 mM KCl, 10 mM Na_2HPO_4, and 1.9 mM KH_2PO_4, pH 7.4.

2.2. Synthesis of polymers

2.2.1. Synthesis of PEG6kDA macroinitiator

PEG was functionalized with α-bromoisobutyrylbromide to yield an ATRP macroinitiator using a procedure described by De Graaf et al. [51] Briefly, dehydrated PEG 6 kDa (10.0 g) was dissolved in 100 mL dry THF at 50 °C under a nitrogen atmosphere. Triethylamine and α-bromoisobutyrylbromide were added (1.5 eq to the hydroxyl groups). The mixture was stirred overnight at room temperature. The formed TEA

bromide salt was filtered off and the filtrate was concentrated under vacuum, subsequently dissolved in water (20 mL) and centrifuged (5500 *g*, 5 min, 25 °C). The supernatant was filtered with a filter paper and the filtrate was dialyzed (3.5 kDa MWCO) against water for two days and then freeze-dried. The product dissolved in $CDCl_3$ was characterized by ^{1}H NMR spectroscopy. ^{1}H NMR analysis showed the formation of a fully functionalized PEG ATRP macroinitiator. ^{1}H NMR ($CDCl_3$): $\delta = 4.3$ (t, 4H, OCH_2), 3.85 (t, 4H, OCH_2), 3.65 (t, 531H,OCH_2), 3.35 (t, 4H, OCH_2), 1.85 ppm (s, 12H, CCH_3). The absence of PEG hydroxyl groups was confirmed by adding two drops of trichloroacetyl isocyanate (TAIC) to the NMR sample to react with possible present unmodified OH groups [52].

2.2.2. Synthesis of P(NIPAM-co-HEA)-PEG-P(NIPAM-co-HEA) (PNH)

PEG 6 kDa macroinitiator (500 mg; 0.083 mmol) was dissolved in 20 mL H_2O. Subsequently, NIPAM (2.54 g; 22.5 mmol), CuBr (50 mg; 0.35 mmol) and 2-hydroxyethyl acrylate (HEA) (280 μL; 2.4 mmol) were added and dissolved. The solution was deoxygenated by flushing with nitrogen gas for 15 min at room temperature and additionally 15 min on ice. The reaction was started by adding tris[2-(dimethylaminoethyl] amine (Me6-TREN) (90 μL; 0.34 mmol) to the reaction mixture, which resulted in a colour change from colorless to green/blue. The reaction was carried out for three hours on ice under nitrogen atmosphere. The reaction mixture was subsequently dialyzed against water for 48 h at 4 °C (dialysis tube MWCO 6–8 kDa, Thermo Scientific, Bleiswijk, the Netherlands). The product as white powder was obtained after freeze drying and is further named as PNH. The polymer molecular weight was determined by ^{1}H NMR and GPC. ^{1}H NMR spectrum of PNH in D_2O. δ (ppm): 1.13 (6H, CH_3CHCH_3, NIPAM); 1.30–2.30 (backbone hydrogens); 3.68 (545H, CH_2OCH_2, PEG); 3.78 (2H, CH_2OCO, HEA); 4.20 (2H, CH_2OH, HEA); 3.87 (1H, CH_3CHCH_3, NIPAM); 4.79 (D_2O).

2.2.3. Synthesis of P(NIPAM-co-HEA/Maleimide)-PEG-P(NIPAM-co-HEA/Maleimide) (PNM)

PNH (1.00 g; 0.023 mmol, 43.5 kDa) was dissolved in 20 mL dry DCM by stirring for 30 min on ice under nitrogen atmosphere. N,N′-dicyclohexylcarbodiimide (DCC) (107 mg; 0.52 mmol), 4-(dimethylamino)pyridine (DMAP) (0.64 mg; 0.0052 mmol) and 6-maleimidohexanoic acid (110 mg; 0.52 mmol) and thus 0.63 eq of HEA in PNH can potentially be modified) were added and the mixture was stirred for 1 h on ice. Next, the reaction mixture was stirred for 16 h at RT, and the formed product was collected by filtration after dropping the reaction mixture in cold diethyl ether. The precipitate was subsequently dissolved in 50 mL H_2O, the remaining solid was filtered off using a 0.45 μm syringe filter, and the filtrate was freeze-dried overnight. The obtained product, further named PNM, was collected as a white powder.^{1}H NMR spectrum of PNM in $CDCl_3$: δ (ppm) 1.13 (6H, CH_3CHCH_3, NIPAM); 1.30–3.0 (backbone hydrogens); 3.68 (4H, OCH_2CH_2O, PEG); 4(1H, CH_3CCH_3, NIPAM); 4.23 (4H, OCH_2CH_2O) 6.71 (2H, maleimide); 7.26 ($CDCl_3$).

2.2.4. Synthesis of P(NIPAM-co-HEA/Furan)-PEG-P(NIPAM-co-HEA/Furan) (PNF)

PNH (1.00 mg; 0.023 mmol, 43.5 kDa) was dissolved in 25 mL $CDCl_3$ and stirred for 30 min while flushed with nitrogen gas. Next, 3-(2-furyl) propionic acid (73 mg; 0.52 mmol; this mean that 0.63 eq HEA in PNH can potentially be modified), DCC (108 mg; 0.52 mmol) and DMAP (0.64 mg; 0.0052 mmol) were added and the mixture was stirred for 16 h at RT. The reaction mixture was dropped in cold diethyl ether and the formed precipitate after filtration was subsequently dissolved in 40 mL H_2O. The remaining solid was filtered off using a 0.45 μm syringe filter, the filtrate was freeze-dried overnight, and the product, further named PNF, was collected as a white powder. ^{1}H NMR spectrum of PNF in $CDCl_3$: δ (ppm) 1.13 (6H, CH_3CHCH_3, NIPAM); 1.30–3.0 (backbone hydrogens); 3.68 (4H, OCH_2CH_2O, PEG 6 kDa); 4.0 (1H, CH_3CCH_3, NIPAM); 4.23 (4H, OCH_2CH_2O) 6.01 (1H, CCHCH, Furan); 6.26 (1H, CHCHCH, Furan); 7.29 (1H, CHCHO, furan); 7.26 ($CDCl_3$).

2.3. Polymer characterization

2.3.1. ^{1}H NMR spectroscopy

The synthesized polymers were characterized with ^{1}H NMR spectroscopy using a Bruker 600 Hz MR-NMR spectrometer (Bruker BioSpin GmbH). Data analysis was performed using MestReNova Software. The chemical shifts are referred to the residual solvent peak ($\delta = 7.26$ ppm for $CDCl_3$ and $\delta = 4.80$ ppm for D_2O).

2.3.2. Cloud point determination

Samples of the thermosensitive polymers were dissolved in PBS at a concentration of 3 mg/mL. The cloud point (CP) was measured using a Jasco FP-8300 spectrophotometer (JASCO, Easton, MD) with a water-cooled Peltier thermostatted 4-position automatic cell changer. The Spectra Manager program was used for measuring scattering at a wavelength of 650 nm while the temperature was raised from 4 to 40 °C at a rate of 1 °C.min^{-1}. The onset point of increased scattering intensity is reported as CP [53].

2.3.3. Rheological characterization

The rheological properties of the formulations were studied using a Discovery HR-2 Rheometer (TA Instruments Inc., Etten-Leur, the Netherland) with a Peltier Plate for temperature control and solvent trap to prevent evaporation of the solvent. Empty and drug loaded PNF-PNM hydrogel formulations with different polymer concentrations (5, 10, 15 wt%) were prepared as described in section 2.4., after mixing the polymer/drug solutions, the resulting solution was placed under the geometry and measured using a plate-plate geometry (aluminum, 20 mm diameter, initial gap was 200 μm). Normal force was controlled during the experiments to enable measurements of samples while volume changes occur. Data were processed using TRIOS Software version 5.0. The storage (G') and loss (G") moduli were measured during a temperature ramp ranging from 4 up to 37 °C at a rate of 0.5 °C.min^{-1} and at a strain 0.5%. Next, the sample was kept at 37 °C for 30 min and then a frequency sweep ranging between 0.1 and 100 rad.s^{-1} was performed at strain 0.5%. The samples were then cooled down from 37 to 4 °C at a rate of 0.5 °C.min^{-1}. From the average G' at 37 °C, the mesh size (ξ in m) of the formed hydrogels was calculated according to the following equation [54], using Avogadro's number (N_{av}) in mol^{-1}, R the molar gas constant in J.K^{-1}.mol^{-1}, and the temperature (T) in K and G' in Pa:

$$\xi = \left(\frac{G'^{*}N_{av}}{RT}\right)^{-1/3}$$

2.3.4. FTIR analysis

Fourier Transform Infrared (FTIR) spectra were measured for the PNF and PNM polymers and for a dried 10 wt% PNF-PNM hydrogel. The samples were measured as dried solid powers. The spectra, ranging from 600 cm^{-1} to 4000 cm^{-1}, were recorded with a Perkin Elmer Spotlight FT-IR Spectrometer.

2.3.5. Gel permeation chromatography

Polymer samples were dissolved in the eluent, 10 mM LiCl in DMF, at a concentration of 3 mg/mL. The number average molecular weight (M_n) and polydispersity index (PDI) were determined through gel permeation chromatography (GPC), using a Waters 2695 Alliance (Waters Corporation, Milford, MA) with refraction Index detector and with a PLgel 5 μm Mixed-D column. The analysis was performed with the column set at 65 °C and 1 mL/min flow rate. Empower software was used for data analysis. A calibration curve was obtained by measuring PEG standards of narrow molecular weight (Polymer Standard Service GmbH, Mainz, Germany).

2.3.6. DMA characterization

DMA 2980 Dynamic Mechanical Analyzer (TA-Instruments, Etten-Leur, the Netherlands) was used to determine Young's modulus of the hydrogels as previously reported [38] Thermosensitive DA hydrogel samples were prepared as described in section 2.4.1. The gels (diameter 2.6 mm, 5.2 mm height) were placed between the parallel plates, and a force ramp was applied at a rate of 0.5 N/min up to a total force of 8 N at room temperature. The obtained data were analysed using TA Universal Analysis software and the Young's modulus (E) was calculated from the slope of the linear section of the stress-strain curve. Data are reported as mean ± standard deviation ($n = 3$).

2.4. Preparation of PNF-PNM hydrogels

2.4.1. Non-loaded PNF-PNM hydrogels

PNF and PNM were separately dissolved in PBS (pH 7.4) on ice. The concentrations ranged from 3 to 20 wt% (except when mentioned otherwise). To obtain hydrogels, PNF and PNM solutions were mixed (weight ratio PNF/PNM 1:1, molar ratio furan/maleimide 1:1) to obtain 80 mg hydrogel formulation (except when mentioned otherwise) at the desired total polymer concentration (3–20 wt%). To form the gels, the polymer solutions were incubated in cylindrically shaped plastic moulds (diameter 4.5 mm, 5 mm height) at 37 °C for 3 h (to allow full chemical DA crosslinking). During the incubation at 37 °C, the gels shrunk and expelled some liquid. After gel formation, the gels were transferred into glass vials for further use, either including expelled liquid (for release experiments) or excluding expelled liquid (for degradation experiments).

2.4.2. Preparation of FAB loaded PNF-PNM hydrogels

FAB antibody (3.1 mg/mL) biosimilar to Lucentis® (Ranibizumab) was received from Boehringer Ingelheim, Germany. This FAB antibody is a FAB fragment of the monoclonal antibody Bevacizumab expressed in E.coli. with a mass of 48.4 kDa. The protein was delivered in a mixture of two buffers, 54 (v/v) % buffer 1 (20 mM (CH_3COONa), 8.5 mM (CH_3COOH), 1.1 N $(NH_4)_2SO_4$, pH 5.0) and 46 v/v % buffer 2 (20 mM (CH_3COONa), 10.5 mM (CH_3COOH), pH 5.0). This buffer solution was exchanged by PBS using a ZebaTM Spin Desalting Column (7 K MWCO, Thermo Scientific) and a 2.53 mg/mL PBS FAB antibody solution was obtained (concentration determined by SEC ULPC). FAB loaded hydrogels were prepared according to section 2.4.1 with some modifications. Different gel concentrations (5–20 wt%) were prepared by weighing equal amounts of PNM and PNF, which were separately dissolved (at 4 °C within <2 h) in PBS (volume adjusted based on final polymer concentration) and in PBS containing FAB antibody (48 μL, 2.53 mg/mL), respectively. The obtained PNF-FAB /PNM solutions were mixed to form 80 mg hydrogel formulations (ratio 1:1 furan/ maleimide) and incubated in cylindrically shaped plastic moulds (diameter 4.5 mm, 5 mm height) at 37 °C for 3 h (to allow full chemical DA crosslinking) to obtain a PNF-PMN hydrogels loaded with 121 μg FAB protein.

2.4.3. Preparation of dexamethasone loaded PNF-PNM hydrogels

Dexamethasone-loaded hydrogels of 80 mg were prepared according to section 2.4.1. Briefly, a dex-PBS dispersion was obtained by sonicating 15.98 mg dexamethasone in 960 μL PBS for 10 s before use. Next, equal amounts of PNF and PNM were separately dissolved in PBS (volume adjusted based on final polymer concentration) and in dex-PBS (24 μL, 16.67 mg/mL) respectively, on ice. The PNF solution was mixed with the PNM-dex suspension to obtain a total polymer concentration of 3, 10, or 20 wt% (molar ratio 1:1 furan/ maleimide) unless indicated otherwise.

The PNM-dex dispersion was heated to 37 °C for 15 min prior to mixing with the cold PNF PBS solution. The mixture was transferred into cylindrically shaped plastic moulds (diameter 4.5 mm, 5 mm height) and incubated for 3 h (to allow full chemical DA crosslinking) at 37 °C to obtain a PNF-PMN hydrogel loaded with 400 μg dexamethasone.

2.5. Swelling and degradation characteristics of PNF-PNM hydrogels

2.5.1. Swelling and degradation of PNF-PNM hydrogels in PBS buffer (pH 7.4)

Empty PNF-PNM hydrogels with different concentrations (5, 10, 15 wt%) were prepared as described in section 2.4.1 ($n = 3$). The polymer solutions were transferred into a cylindrically shape plastic mould and the samples were incubated for 3 h (to allow full chemical DA crosslinking) at 37 °C. Only the hydrogels (without the expelled fluid, see below Fig. 1) were removed from the mould and weighed in a glass vial after which 1 mL PBS (pH 7.4) was added and the gels were incubated at 37 °C. To determine swelling and degradation of the hydrogels, at different time points the supernatant was removed and the gel was weighed at room temperature. Afterwards, 1 mL fresh PBS was added. The swelling ratio of the hydrogel at a certain time point is defined as the weight (W_t) divided by the initial hydrogel weight (W_0).

2.5.2. Swelling and degradation of PNF-PNM hydrogels in BBS and PB buffer (pH 10 and 11)

Empty hydrogels (5 wt%) were prepared ($n = 3$) as described in section 2.4.1. The formed hydrogels were removed from the mould and transferred into glass vials and weighed. Next, 1 mL of either borate buffered saline (BBS) (pH 10; 0.01 M H_3BO_3, 0.04 M KCl, 6 mM NaOH) or phosphate-buffer (PB) (pH 11; 0.138 M Na_2HPO_4, 61.8 mM Na_3PO_4) was added and the samples were incubated at 37 °C. Subsequently, at multiple time points, the buffer was removed and the gels were weighed and the swelling ratios were determined as described in (section 2.5.1).

2.6. Drug release from PNF-PNM hydrogels

2.6.1. FAB release from PNF-PNM hydrogels

Fab-loaded hydrogels were prepared as described in section 2.4.2. The crosslinked gels together with the expelled fluid were transferred into glass vials, and subsequently 300 μL PBS with 0.02% NaN_3 (to prevent bacterial growth) was added and the vials were incubated at 37 °C. Note that the time point at which 300 μL PBS was added is considered as $t = 0$ for the release studies as depicted schematically in Fig. 1. However, FAB had partially been expulsed (approximately, 14, 35, 52 μL for 5, 10, 20 wt% gels, respectively) from the hydrogels during the 3 h incubation in the oven. The liquid which was expelled during this 3 h oven treatment was mixed with the 300 μL PBS release medium. Release samples were taken by replacing 200 μL PBS from the vials with 200 μL of pre-warmed fresh PBS (37 °C) at multiple time points. The release samples were stored at 4 °C (company recommended storage conditions) until analysis was performed. To determine the protein concentration, the samples were spun down at 2000 *g* for 5 min and 100 μL of the supernatant was taken for analysis using SE-ULPC on an ARC Acquity UPLC (Waters Corporation, Milford, USA) with an FLR-detector, operated at λ_{ex} and λ_{em} of 280 and 310 nm, respectively. Results were analysed with Empower Software (Version 3-FR5). A calibration curve was obtained by analyzing solutions of FAB in PBS (from 1.2 to 2600 μg/mL). The standard samples (7.5 μL) and the release samples (7.5 μL) were injected onto Phenomenex BioSep-SEC-S2000 (300 × 7.80 mm) column and the eluent was 0.3 M sodium sulphate with 100 mM sodium phosphate monobasic monohydrate buffer (pH 6.7). The system was operated at a flow rate of 0.3 mL/min and the run time per sample was 25 min.

2.6.2. Dexamethasone release from PNF-PNM hydrogels

After preparation of the different dex-loaded hydrogels ($n = 3$, see section 2.4.3), the gels together with the expelled fluid were transferred into glass vials and 300 μL PBS with 1 % tween (to solubilize released dexamethasone) and 0.02% NaN_3 (to prevent bacterial growth) were added to the gels, which were subsequently incubated at 37 °C. Note that, as for FAB, the time point of adding 300 μL PBS is considered as $t = 0$ for the release studies. The liquid which was expelled during this 3 h

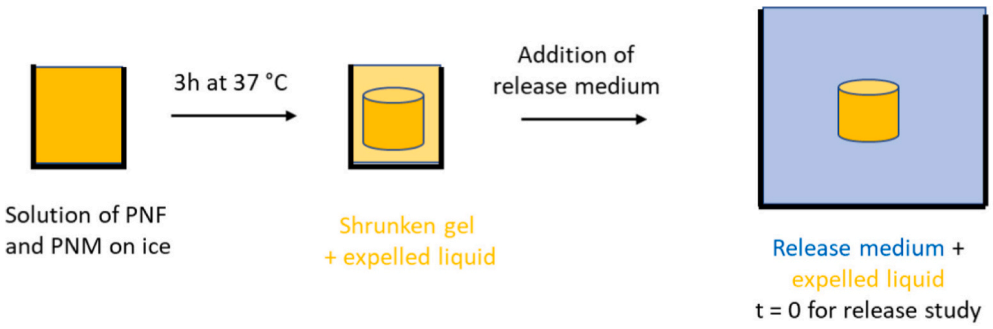

Fig. 1. Schematic overview of the experimental setup of the gel formation and subsequent release study, the expelled liquid indicates the water that was expelled from the gels during shrinking.

oven treatment was mixed with the 300 μL PBS release medium. At different time points samples of 200 μL were taken and replaced with the same volume of fresh PBS/Tween buffer. The dissolution rate of dexamethasone particles in the release medium was also determined. In detail, a dispersion of dexamethasone crystals in PBS (16.6 mg/mL) was sonicated for 10 s. Subsequently, 30 μL of this dispersion was mixed with 300 μL PBS with 1 % tween and incubated at 37 °C. At different time points the dispersion was spun down (at 25,000 *g* in RT for 15 min) and 200 μL of supernatant was taken and replaced by the same volume of PBS with 1 % tween with 0.02% NaN_3. To 100 μL of the release samples or dissolution samples, 10 μL DMSO was added to ensure full solubilization of the released dexamethasone. Subsequently, the samples were spun down again at 25,000 *g* for 15 min. Samples of the supernatant (60 μL) were analysed using Acquity UPLC (Waters Corporation, Milford, MA) equipped with UPLC CSH C18 column (100 × 2.1 mm, 1.7 μm, 130 Å, Waters Corporation). Dexamethasone was detected at 246 nm and quantification was done using a calibration curve of 0.5 to 400 μg/mL dexamethasone in 100 % acetonitrile (ACN). Gradient mobile phase was prepared using 5 % ACN in water as eluent A and 100 % ACN as eluent B, both containing 1 % perchloric acid as pH modifier. Samples of 5 μL were injected, the was flow rate 0.75 mL/min and the gradient run from 0 to 100 % B in 10 min. Results were analysed using Empower Software (Version 3-FR5, Waters Corporation, USA).

2.7. FAB integrity upon incubation with PNF and PNM in buffer and after release from PNF-PNM hydrogels

2.7.1. FAB integrity upon exposure to PNF and PNM polymers

To investigate whether the integrity of FAB upon exposure to PNF and PNM was affected, SDS-PAGE analysis was used. PNF and PNM were separately dissolved in PBS (2 mg/mL) on ice. Subsequently, 50 μL FAB in PBS (2.52 mg/mL) was added to 50 μL solutions of PNF and PNM, and the obtained samples were incubated at 4 and 37 °C for 3 h and for 13 days. As control, FAB was also incubated with 4arm-PEG10K-Maleimide (PEG-Mal; obtained from JenKem Technology, USA) in PBS at the same concentration and conditions. After incubation, 4 μL samples were withdrawn. Next, 18.5 μL of PBS and 7.5 μL of solution of 250 mM Tris-HCl pH 6.5 also containing 8 % sodium dodecyl sulphate (SDS) 0.008 % (*v*/v) Bromophenol Blue; and 40 % (v/v) glycerol with and without β-mercaptoethanol 5 % (100 mM) were added. Hereafter, the samples and controls were heated for 10 min at 90 °C to denature FAB. Subsequently, 28 μL of the samples and 5 μL of the PageRulerTM Prestained Protein ladder (Thermo Fischer Scientific) were pipetted into the Bolt 4–12% bis-tris-plus gel (Thermo Fischer Scientific) that was run in a Bolt MOPS SDS running buffer (Thermo Fischer Scientific) at 100- V for 1 h. The proteins in the gel were stained with Coomassie blue (Thermo Fischer Scientific) overnight and washed in demineralized water before imaging the SDS gel.

2.7.2. FAB integrity after release from PNF-PNM hydrogels

FAB loaded hydrogels were prepared as described in section 2.4.2 and the release of the protein was studied as in section 2.7.1. The integrity of the released FAB from the PNF-PNM hydrogels was investigated using SDS-PAGE as in section 2.8.1. SDS (7.5 μL) was added to 22.5 μL of the FAB release samples taken after 1 h, 1 day and 6 days.

2.8. Cytocompatibility of PNF and PNM

2.8.1. RAW 264.7 cell culture

RAW 264.7 macrophage-like mice cells (catalogue number TIB-71, ATTC, Manassas, VA, USA) were cultured in humidified conditions at 37 °C and 5 % CO_2 with high glucose Gibco Dulbecco's Modified Eagle Medium (DMEM) (Sigma Aldrich, Zwijndrecht, the Netherlands) with 10 % heat-inactivated fetal bovine serum (GibcoTM Thermo Fischer scientific). Cells between passage numbers 15 and 20 were used. The cells were detached from the culture flask using a cell scraper and subsequently counted with a TCTM automated cell counter (Biorad). Next, the cells were seeded in a flat bottom Greiner CellStar 96-well plate (#665090; GreinerBio-One GmbH, GE) at a density of 100,000 cells/cm^2 and allowed to attach overnight prior to experiments.

2.8.2. ARPE-19 cell culture

Human retinal pigment epithelium derived ARPE-19 cells (catalogue number CRL 2302, ATTC) were cultured in humidified conditions at 37 °C and 5 % CO_2 with high glucose Gibco Dulbecco's Modified Eagle Medium/Nutrient Mixture F-12 (DMEM/F12) with 10 % FBS and 1 % L-glutamine. Cells between passage numbers 13 and 20 were used, detached from the culture flask using a trypsin EDTA solution and counted with a TCTM automated cell counter (Biorad). Next, the cells were seeded in a flat bottom polystyrene 96-wells plate at a density of 32,000 cells/cm^2 and allowed to attach overnight prior to experiments.

2.8.3. Alamar blue cytotoxicity assay on RAW 264.7 and ARPE-19 cells exposed to the polymers PNF and PNM

After cell culture (see section 2.8.1 and 2.8.2), the cell medium was refreshed and the cells were incubated with 100 μL complete cell culture medium containing PNF or PNM (concentration from 0 to 5 mg/mL ($n = 3$)). After 24 h incubation at 37 °C, the medium was refreshed and 10 μL of AlamarBlue reagent (500 μM Resazurin sodium salt (Sigma-Aldrich) in PBS) was added per well. It is noted that the medium was cloudy due to polymer precipitation at 37 °C. As a negative control, the medium of 3 wells was replaced with complete cell culture medium containing 1 % Triton X-100 to lyse the cells. After 15 min, 10 μL of the AlamarBlue reagent was added. Three empty wells were also filled with 100 μL medium and 10 μL AlamarBlue reagent was added to correct for the background. The 96-wells plates were incubated for 3 h at 37 °C protected from light. The fluorescence was measured using a Fluostar OPTIMA (BMG Labtech GmbH, Ortenberg, Germany) plate reader with a fluorescence excitation wavelength of 550 nm and an emission

wavelength of 590 nm. After background correction, the fluorescence intensities were normalized to the intensities of cells cultured in medium without polymers.

2.8.4. Live-dead staining of RAW 264.7 and ARPE-19 cells exposed to the polymers PNF and PNM

Cells seeded in a flat bottom glass 96-wells plate (Greiner CellStar 96-well plate #655090) were cultured as described in section 2.8.1 and 2.8.2. The cells were incubated in medium containing PNF or PNM (0 to 5 mg/mL) ($n = 2$) in humidified conditions at 37 °C and 5 % CO_2 for 24 h. Because the medium was cloudy due to precipitation of the polymer, it was replaced by 100 μL medium containing 3 μM Calcein AM (Cayman Chemical Company, MI, USA) and 25 μM propidium Iodide (PI) (Invitrogen Thermo Fisher Scientific). As negative control, medium of 3 wells was replaced by medium containing 1 % Triton X-100 to lyse the cells. After 15 min, the medium was replaced by 100 μL medium containing 3 μM Calcein AM and 25 μM PI. The cells were incubated for at least 5 min before imaging. Minimal 3 images were made using a Yokogawa Cell Voyager 7000 Spinning Disconfocal Microscope with a fluorescence emission wavelength of 525 nm to visualize the living cells and 600 nm for the dead cells. The images were further processed with *ImageJ* processing software and the living and the dead cells were counted using *Columbus* processing software.

2.8.5. Life-dead staining of RPE-19 cells in direct contact with PNF-PNM hydrogels

Human retinal pigment epithelium cells were cultured in a flat bottom glass 12-wells plate (Greiner CellStar glass bottom 24-well plate, #662892) in 500 μL DMEM/F12 (52,000 cells/cm^2) as described in section 2.8.2. Before cell seeding, a 10 wt% PNF-PNM solution (50 μL) was placed in the corner of the well, and the hydrogel was formed upon incubation for 3 h at 37 °C. After culturing cells with the PNF-PNM hydrogel for 24 h in the wells, a life-dead staining was performed. In short, 100 μL medium was removed and replaced by 50 μL medium containing 30 μM Calcein AM (final concentration 3 μM) and 50 μL medium containing 250 μM PI (final concentration 25 μM). As negative control, 50 μL medium of 3 wells was replaced by 50 μL medium containing 1% Triton X-100 to lyse cells. After 15 min, Calcein AM and PI were added according to the protocol described above. Images were made and processed according to section 2.8.4.

2.9. Video: Intravitreal injection of PNF-PNM hydrogel on an ex vivo rabbit eye

The eyeball from a rabbit cadaver was enucleated within one hour after animal termination. The eye was dissected using a scalpel to make an incision and a towel forceps to ensure control and stability. First, the eyelids of the eye that was enucleated were opened and stabilized by clamping them to the skin. An incision was made on the skin with a scalpel at the nasal and temporal side of the eye by making solid lines. Subsequently, after removing the towel forceps, an incision on the skin and periocular tissues by moving the scalpel parallel to the orbital rim was made. At this point, the eyelids were still attached to the anterior part of the eye. Therefore the eyeball was slightly pulled out of the orbital cavity with the help of a towel forceps, the optic canal in the sphenoid bone was located by touch, and the optic nerve was dissected as deep as possible. Finally, any other remating periocular tissues surrounding the eye inside the orbital cavity (muscles, connective tissues) were dissected, and the eyeball was entirely pulled out of the orbital cavity. The enucleated eye was stored in PBS buffer (pH 7.4) at 0 °C to arrest the metabolic activity of the tissues. Prior to the intravitreal injection, the eyeballs were incubated at 37 °C for 30 min in a water bath. Hydrogel formulations of 10 wt% were chosen to assess if the formulation with the lowest used concentration is able to form a stable gel in an ex vivo setting. Therefore, PNF-PNM (10 wt%, 50 μL) samples were prepared as described in section 2.4.1 and injected into the vitreous body of the rabbit eye using a syringe with a 30 G needle. After injection, the eye was incubated at 37 °C for 3 h (to allow full chemical DA crosslinking), after which an incision was made to expose the vitreous body and to visualize the in situ formed hydrogel.

3. Results & discussion

3.1. Polymer synthesis and characterization

Fig. 2 shows the synthesis scheme of the two complementary polymers, PNF and PNM, containing respectively furan and maleimide functional groups. TAIC assay demonstrated that both terminal hydroxyl groups of PEG with a number average molecular weight (M_n) of 6 kDa were quantitively functionalized with bromoisobutyryl bromide groups to yield a PEG macroinitiator. The macroinitiator was subsequently used to copolymerize HEA and NIPAM through ATRP-polymerization to obtain PNH, an ABA triblock copolymer as shown in Fig. 2A. The B-block consists of PEG for its hydrophilic properties whereas the outer A-blocks consist of two monomers, NIPAM, to render the polymer thermosensitive, and HEA, to enable post-modification of the thermosensitive block via coupling on its hydroxyl group. The PNH triblock copolymer after dialysis and lyophilization was obtained with a yield of 90–95 %. Its chemical composition was confirmed by ^{1}H NMR analysis (see SI-fig. 1A). The molar feed ratio of NIPAM/HEA was 90:10 (Table 1), and a ratio of 88:12 of the copolymers was measured by ^{1}H NMR analysis. Therefore, within the experimental error for NMR analysis, the composition of the thermosensitive A block equals the feed ratio, which is expected since the synthesized polymer was obtained in a high yield. The obtained polymer had an M_n of 43 kDa as determined by ^{1}H NMR analysis and of 33 kDa as determined by GPC with a polydispersity index (PDI) of 1.7. (Table 1). The cloud point (CP) of PNH as determined by light scattering was 32 °C (SI-fig. 2), which is in accordance with literature data for block copolymers containing PNIPAM rich blocks [55,56]. To allow Diels-Alder crosslinking, 67% (feed ratio) of HEA groups in PNH were functionalized with either 3-(2-furyl)propionic acid or 6-maleimidohexanoic acid via DCC/DMAP coupling to obtain the two complementary thermosensitive triblock polymers PNF and PNM, respectively, as shown in Fig. 2B, C. The esterification of the HEA moieties was confirmed by ^{1}H NMR (see SI-Fig. 1B, C) which showed a ratio 88:4:8 between NIPAM, residual HEA and furan or maleimide moieties respectively for PNF or PNM (Table 1). These results show that the esterification was quantitative. The M_n of the synthesized polymers was determined by ^{1}H NMR and GPC analysis. Results showed that PNF had an M_n of 44 kDa (^{1}H NMR) and 38 kDa (GPC) while PNM had an M_n of 46 kDa both by ^{1}H NMR and GPC. The PDI of the polymers were between 1.6 and 2.2. As expected, the CP of PNF and PNM slightly decreased from 32 to 28 and 29 °C respectively, as PNM and PNF are more hydrophobic than PNH.

3.2. Hydrogel formation and characteristics

Fig. 3A (left column) shows vials containing aqueous solutions of either a mixture of PNF and PNM or the separate polymers directly after dissolution at 4 °C. Subsequently, incubation of the polymer solutions (mixture of PNF/PNM, PNF, PNM) for 2 h at 37 °C (Fig. 3A, middle column) resulted in viscous opaque solutions for the individual polymers due to physical self-assembly of the PNIPAM domains. On the other hand, the PNF-PNM mixture under the same conditions formed an opaque gel that lacked flow upon tilting the vial upside down (Fig. 3A, middle column).

Fig. 3A (right column) shows that upon cooling down the samples to 4 °C resulted again in clear liquid solutions for both PNF and PNM. This means that reversible physical interactions are responsible for the change in visual appearance and gel formation of the PNF and PNM systems upon incubation at 37 °C. Importantly, and in contrast, upon cooling to 4 °C, the PNM-PNF mixture remained a gel, which strongly

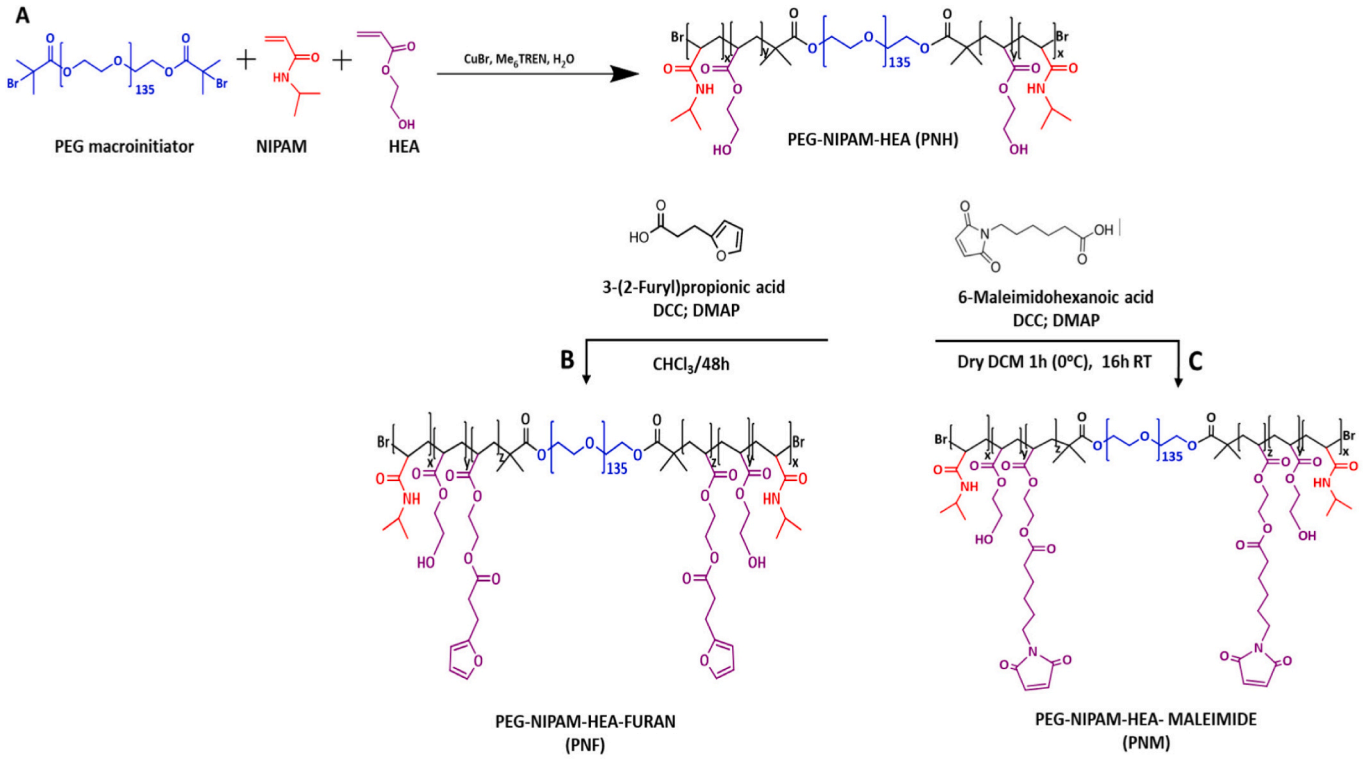

Fig. 2. A) Synthesis of PNH by ATRP polymerization and its functionalization with B) 3-(2-furyl)propionic acid resulting in PNF, and C) with 6-maleimidohexanoic acid resulting in PNM.

Table 1
Characteristics of the three ABA triblock copolymers (PNH, PNF and PNM) composed of PEG mid-block of 6 kDa with outer blocks of NIPAM (N) and HEA (H) or furan (F) or maleimide (M).

Polymer	Feed Ratio [N]:[H]:[F]/[M]	Measured Ratio[a] [N]:[H]:[F]/[M]	M_n [a] (kDa)	M_n [b] (kDa)	PDI [b]	Cloud Point [c] (°C)
PNH	90:10:NA	88:12:NA	43	33	1.7	32
PNF	88:4:8	88:4:8	44	38	1.6	28
PNM	88:4:8	88:4:8	46	46	2.2	29

[a] Determined by ^{1}H NMR.
[b] Determined by GPC.
[c] Determined by light scattering.

suggests that DA crosslinking indeed had occurred after the physical crosslinking and subsequent incubation at 37 °C.

Furthermore, scanning electron microscopy (SEM) analysis was performed to examine the microstructure of freeze-dried drug-loaded hydrogels and compare it with that of empty hydrogels. SI-Fig. 10 shows different pore-type structures at three magnifications. Empty hydrogels exhibited small, interconnected pores, while FAB protein-loaded hydrogels had larger pores with smaller interconnected pores. Dex-loaded hydrogels displayed heterogeneous microstructures with zones of lamellar structures and flat surfaces with smaller pores.

3.2.1. *Rheological characterization*

Rheological studies were performed to study the gelation kinetics, the reversibility of both the PNF-PNM formulation and individual polymer solutions upon heating and cooling and the stiffness of the formed PNM-PNF hydrogels.

The temperature at which G′ (storage modulus) crosses G″ (loss modulus) is defined here as the gelation temperature (T_{gel}). The PNF-PNM formulation showed a T_{gel} at 23 °C, while the solutions of the individual PNF and PNM solutions showed a T_{gel} of 24 and 28 °C, respectively (Fig. 3B). The G' of the hydrogels (PNM/PNF, PNM and PNF solutions) progressively increased when the temperature increased from T_{gel} up to 37 °C most likely due to the thermosensitive nature of the polymers.

After 30 min at 37 °C, the gels were stressed at a fixed strain and increasing frequency. It was shown that the G' of the gels based on PNF or PNM increased (for PNM from 38 to 920 Pa, for PNF from 450 to 3200 Pa) with an increasing frequency (SI-Fig. 3A). This is to be expected as only physical crosslinks are present in the gel network. [47,57] In contrast, after 30 min at 37 °C, the PNF-PNM hydrogel showed already a substantial higher G' (2200 Pa) at low frequency compared to the single polymer gels that subsequently increased up 3430 Pa at higher frequency (SI-Fig. 3A). This higher G' of the PNF-PNM formulation suggests that additional chemical crosslinks were formed. In addition, Fig. 3B shows that a decrease in temperature of the separate polymer systems resulted in a decrease of both G' and G" which can be ascribed to the reversible hydration of the pNIPAM blocks of the polymers. The PNM system showed almost reversible behavior during cooling from 37 to 4 °C with a rapid decrease of G', G" (Fig. 3 B1) and complex viscosity (SI-Fig. 3D) between ~30 and 25 °C, while substantial hysteresis was observed for the PNF system (Fig. 3 B2). This might be due to weak heteroaromatic π-π stacking interaction between the furan moieties [58,59] formed above the LCST and still present upon cooling of the gel below this temperature.

Fig. 3 B3, shows that when the PNF-PNM gel was cooled down from 37 to 4 °C, G' remained higher than G" and G' decreased from 3100 to 650 Pa while cooling from 37 to 23 °C, likely because of the loss of the physical crosslinks below the LCST. Subsequently, G' increased up to 3100 Pa at 4 °C, likely because additional DA crosslinks were formed in time.

Drug-loaded PNF-PNM gels were also rheologically characterized. The plateau modulus as a function of angular frequency at 37 °C showed

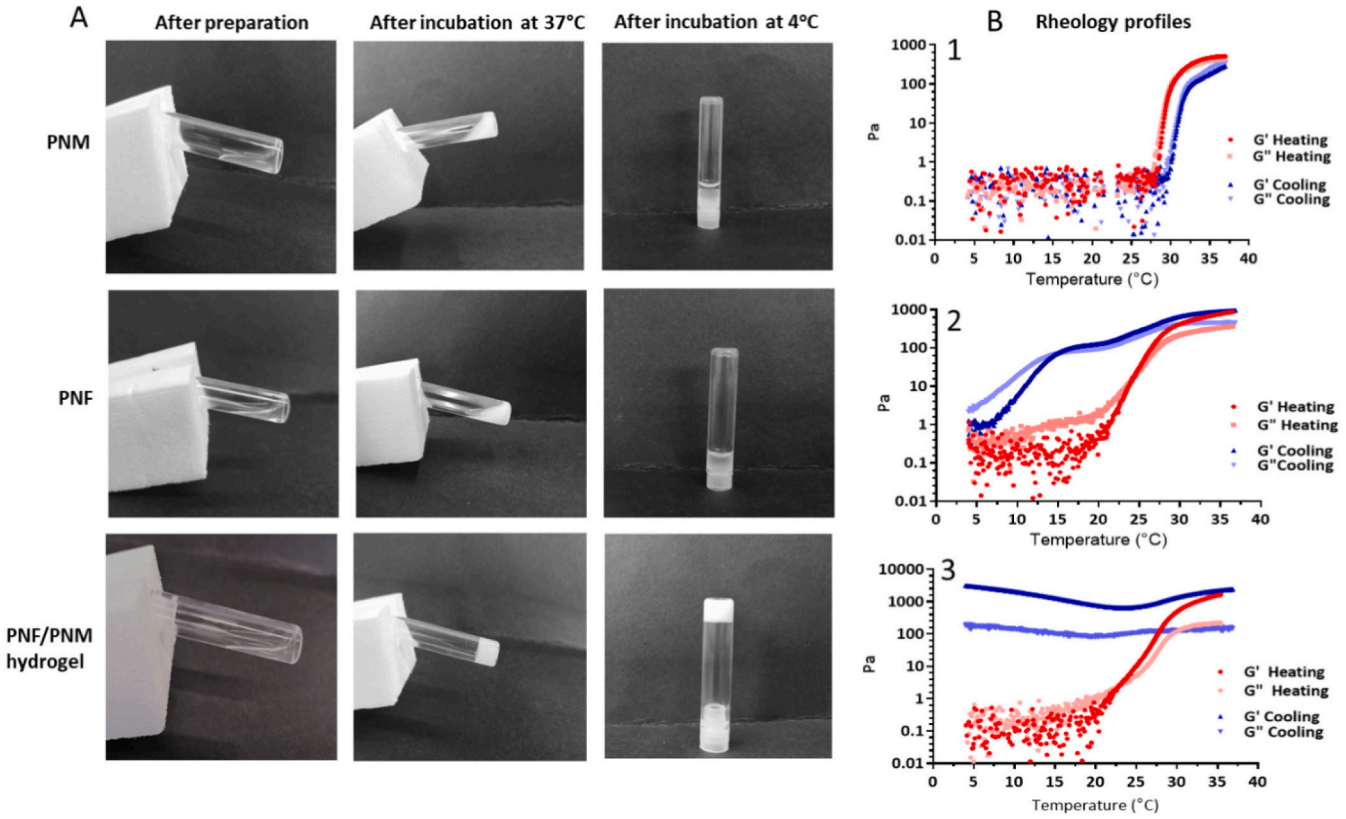

Fig. 3. A) Images of PNF, PNM, and PNF-PNM systems at room temperature shortly after dissolution of the polymers, after incubation at 37 °C for 2 h and cooling down to 4 °C. B) Rheogrammes of PNF and/or PNM polymer systems upon heating (4 to 37 °C) and cooling (37 to 4 °C). B1: PNM 10 wt% polymer, B2: PNF 10 wt% polymer, and, B3: PNF-PNM mixture 10 wt%, at a 0.5 % strain.

only minor differences between FAB-loaded, dex-loaded, and non-loaded gels (SI-Fig. 3 A, B, C). This means that the loaded drugs did not interfere with the polymeric networks. As expected, all gels showed a higher G' with increasing polymer concentration, which points to a higher crosslinking density. The calculated mesh size using the equation mentioned in section 2.3. resulted in a value of 9 nm for 20 wt% gel and 21 nm for the 5 wt% gel (Table 2).

3.2.2. FTIR characterization

FTIR characteristics of the dried hydrogels and polymers were investigated to show DA crosslinking between the furan functionalities of PNF and maleimide functionalities of PNM after incubation in PBS for 3 h at 37 °C. Fig. 4 shows that PNF-PNM hydrogels (A), PNM (B) and PNF (C) absorbed IR light of 1455, 1640 and 1535 cm^{-1}, which can be assigned respectively to the CH_3 bending vibration, the amide I band due to the C═O stretching vibration and amide II band (a combination of the N—H bending and C—N stretching vibration) [60,61] all present in the pNIPAM blocks of the polymers. The absorbance peak at 1737 cm^{-1} is assigned to the C═O stretching vibration of the ester groups present in PNF and PNM and in the hydrogel. Furthermore, the observed broad peaks of the CH_2CH_2 stretching vibrations at 2800–3005 cm^{-1} [62] are ascribed to the PEG blocks of the PNF/PNM polymers and the hydrogel. Additionally, the spectrum of PNM shows peaks at 1707 cm^{-1} and at 695 cm^{-1} which are assigned to the C═O stretch and =C-H- bending vibration of the maleimide group [63,64], while in the spectrum of PNF a peak at 737 cm^{-1} is present which is ascribed to the = C-H- bend vibration of the furan moiety [65,66]. The spectrum of the PNF-PNM hydrogel prepared with a molar ratio maleimide/furan 1:1 (Fig. 4A) clearly showed both the absence of the bending and stretching vibrations at 695 and at 1707 cm^{-1}, characteristic for the maleimide groups, and at 737 cm^{-1}, characteristic for the furan group. The absence of these peaks (indicated by the red arrow in Fig. 4) shows that maleimide and furan moieties present in the PNM and PNF, respectively, were consumed during network formation, demonstrating that DA chemical crosslinking had occurred. It is noted that the absorbance at 1459 cm^{-1} characteristic for the formed DA-adduct [67] was not detected in the hydrogel due to the strong interference of the PNIPAM amide II band and CH_3 bending vibration at 1535 and 1455 cm^{-1}, respectively.

Table 2
G' and mesh size (ξ) of the PNF-PNM hydrogels calculated using equation in section 2.3.3.

hydrogel	G' of FAB loaded gel (kPa)	Mesh size of FAB loaded gel (nm)	G' of Dex loaded gel (kPa)	Mesh size of Dex loaded gel (nm)
5 wt% PNF-PNM	0.38 ± 0.05	22.5 ± 2.8	0.46 ± 0.07	21.0 ± 3.1
10 wt% PNF-PNM	3.13 ± 0.45	11.1 ± 1.6	0.97 ± 0.15	16.4 ± 2.6
20 wt% PNF-PNM	6.16 ± 1.27	8.9 ± 1.8	5.12 ± 1.00	9.4 ± 1.8

3.2.3. Degradation of PNF-PNM hydrogels

During hydrogel formation at 37 °C, a concentration dependent shrinking of the gels occurred, and the 15, 10 and 5 wt% gels lost, respectively, 65, 44 and 17 % of their initial volumes. This means that a higher extent of water expulsion and thus shrinking of the gels occurred with increasing polymer concentration. This is likely due to higher

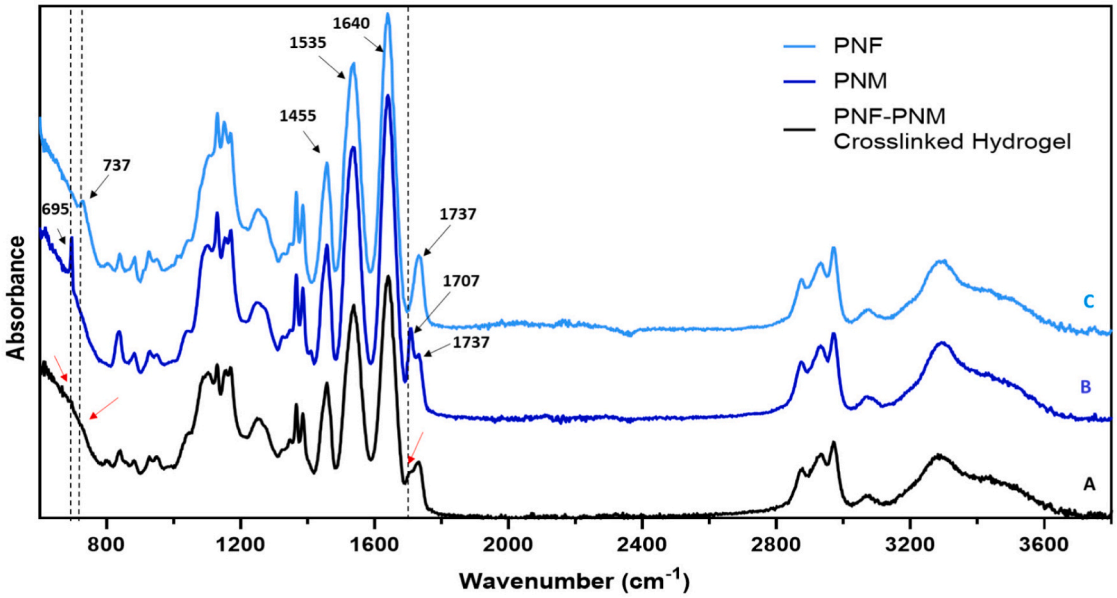

Fig. 4. FT-IR spectra of A) PNF-PNM dried hydrogel (molar ratio 1:1 of furan and maleimide), B) PNM, C) PNF. Black arrows indicate the most relevant peaks and the red arrows point to the disappeared peaks after formation of the chemically crosslinked hydrogel due to DA reaction. (For interpretation of the references to colour in this figure legend, the reader is referred to the web version of this article.)

PNIPAM content of the gel network with increasing polymer concentration in combination with higher concentrations of the functional groups, resulting in both a higher physical and chemical crosslink densities. SI-fig. 5 shows that the hydrogels incubated in PBS at 37 °C remained stable during incubation for >460 days, demonstrating that no significant degradation of the gels occurred.

Ilochonwu et al. and Kirchhof et al. [38,39] reported that DA hydrogels degraded in aqueous solution (PBS pH 7.4) at 37 °C by retro Diels Alder (rDA) reactions to generate furan and maleimide. The degradation of DA crosslink-based hydrogels primarily occurs through the irreversible hydrolytic ring opening of the maleimide group. Surprisingly, under the same conditions, PNF-PNM hydrogels did not degrade even after 460 days. This intriguing result may be attributed to the location of the chemical DA crosslinks within the hydrophobic domains of the hydrogel network. These domains limit water accessibility, thereby slowing down the hydrolysis of maleimide groups. It is worth noting that network degradation can also occur through hydrolysis of the ester bonds that connect the P (PEG) to the NF or NM blocks. Neradovic et al. [68] observed a half-life of 34 h for this ester bond at pH 8.5 and 37 °C in a similar block copolymer. Hence, it can be expected that at pH 7.4 and 37 °C, the half-life would be approximately 340 h. However, as mentioned before, the degradation time for PNF-PNM hydrogels at pH 7.4 is significantly longer. To gain additional insights into the stability and degradation kinetics, 5 wt% PNF-PNM hydrogels were incubated at 37 °C in buffers with pH 10 and 11. This was done to investigate whether hydrolysis can take place under accelerated conditions, either through rDA or ester hydrolysis. SI-fig. 5B shows that the swelling ratio of the gel incubated at pH 11 rapidly decreased and complete degradation was observed after 3 days, while the gel incubated at pH 10 showed slight increase in swelling ratio until complete degradation between day 8 and 13. These results demonstrate that PNF-PNM hydrogels are degradable by hydrolysis, but it is likely a very slow process at neutral pH.

Moreover, it is crucial to consider the presence of degradation enzymes in the vitreous humor in an in vivo situation. Esterases, hydrolases, and other enzymes are present in the vitreous humor and possess the ability to catalyze the hydrolysis of ester bonds within the hydrogel [69]. These enzymes have the potential to actively contribute to the degradation process, thereby influencing both the rate and extent of hydrogel degradation within the vitreous humor.

3.3. Drug release from PNF-PNM hydrogels

3.3.1. FAB release from PNF-PNM hydrogel

Fig. 5 shows that a substantial burst release was observed for the different hydrogels depending on polymer concentration, most likely due to water, and thus also protein, expulsion caused by dehydration of the pNIPAM domains during hydrogel formation and shrinking (Fig. 1). It is intuitively expected that this burst is correlated with the extent of water expulsion. However, this was not observed since the burst was 46, 45 and 28 % for the 5, 10 and 20% hydrogels and thus not proportional to the extent of dehydration (17, 44, 65% for 5, 10, 20 wt% gels, respectively).

It was observed that the storage moduli (see SI-fig. 3) and Young's moduli (see SI-Fig. 4) increased with polymer weight % of the gels pointing to an increase in crosslinking density with smaller mesh sizes (Table 2), which might overall lead to lower burst release of the protein. Fig. 5 further shows that during the first day, protein release was rapid, followed by a subsequent slower release phase during the following 12 days. Fig. 5 also shows that hydrogels with 5 and 10 wt% polymer content showed quantitative release of the loaded protein in 13 days, while the 20 wt% hydrogel released 83 % of the loaded protein during the same time (Fig. 5). The hydrodynamic radius of the FAB protein is 2.7 nm [70] (protein diameter of 5.4 nm) which is smaller than the estimated average mesh size of the hydrogel network (see Table 2). The turbid nature of the PNF-PNM hydrogels indicates that phase separation into polymer- and water-rich areas occurred. As a consequence, protein molecules present in the less densely crosslinked regions of the gel network are mobile and rapidly diffuse out during the first day, whereas in the second phase (day 1–13), protein molecules present in more densely crosslinked zones are released. Similar biphasic release behavior of proteins from phase separated PEG/thermosensitive hydrogels was reported by Censi et al. [71] Likely, in the hydrogel with 20 % polymer, protein molecules are entrapped in cages with pores smaller than the hydrodynamic radius of the FAB restricting protein mobility and resulting in incomplete release.

To more quantitatively evaluate the diffusional mass transport for FAB release, the following analytical solution of Fick's second law was

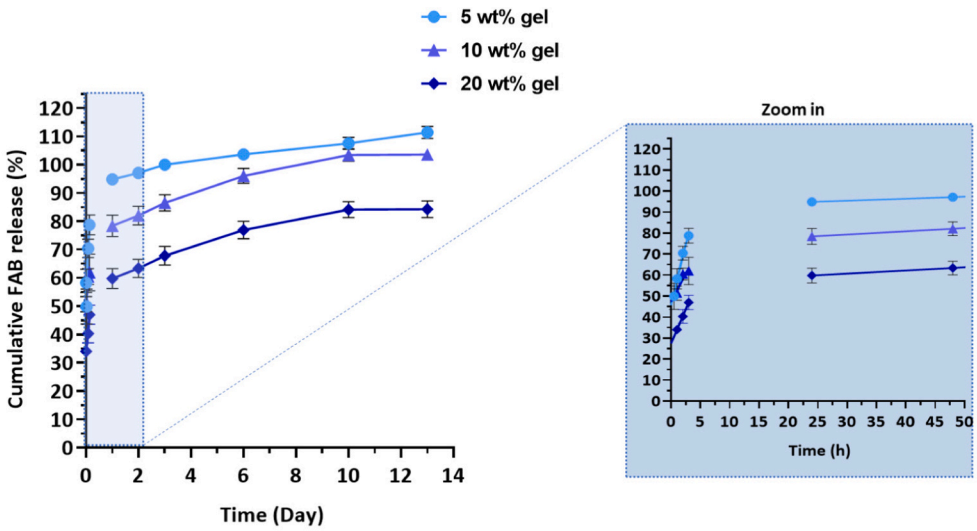

Fig. 5. Cumulative FAB release in PBS at 37 °C from cylindrical PNF-PNM hydrogels with initial polymer concentration of 5, 10 and 20 wt% and diameters of 3.4, 2.3, 1.4 mm and heights of 3.8, 2.6, 1.6 mm respectively. The dimensions of the hydrogels were calculated from their weights after preparation (legend Fig. 4) assuming isotropic deswelling. The data are presented as mean ± SD of three independent replicates. For clarity, at time 300 μl buffer was added to the hydrogels and expelled fluid (see Fig. 1).

applied. [72,73]

$$\frac{M_t}{M_\infty} = 1 - \frac{32}{\pi^2}\cdot\sum_{n=1}^{\infty}\frac{1}{q_n^2}\cdot exp\left(-\frac{q_n^2}{R^2}\cdot D\cdot t\right)\cdot\sum_{p=0}^{\infty}\frac{1}{(2\cdot p+1)^2}\cdot exp\left(-\frac{(2\cdot p+1)^2\cdot\pi^2}{H^2}\cdot D\cdot t\right) \quad (1)$$

where M_t and M_∞ are the cumulative amounts of FAB released at time t and infinity, respectively; n and p are dummy variables; q_n are the roots of the Bessel function of the first kind of zero order [J0(qn) = 0]; D is the apparent diffusion coefficient of the protein in the hydrogel; R and H denote the radius and height of the cylindrical gels. In this study, the experimentally determined release plateau values of FAB (Fig. 5) were considered as amounts released at "infinite" time and thus being the mobile fraction of the loaded protein.

The following boundary conditions apply to the derivation of this equation:

1) Mass transport resistance in the release medium (bulk fluid) is negligible compared to mass transport resistance in the hydrogel.
2) The protein is initially homogeneously and molecularly distributed throughout the gel.
3) FAB transport occurs in radial and axial direction of the cylindrical hydrogel.
4) The diffusion coefficient of the protein is not dependent on time or position.
5) The hydrogel does not dissolve or swell upon exposure to the medium during the release period.
6) Protein release is zero at $t = 0$. Note that this assumption was not fulfilled in the present study since the obtained gels after their preparation including expelled buffer/proteins were transferred in the release medium. Thus this expelled liquid was mixed with the release medium at t = 0.

Fig. 6 shows an example for the fitting of Eq. 1 to experimentally measured FAB release from a hydrogel of 5 % polymer. As it can be seen, the agreement between the fitted curve and actual release data is poor and Eq. 1 systematically underestimates protein release at early time points, and *over*estimates FAB release at late time points. The same observation was made for all other investigated hydrogels, irrespective of the polymer concentration. This poor fit is not unexpected since some of the boundary conditions mentioned above are not valid. Since as pointed out, the hydrogels are likely phase separated systems with water poor and water rich regions, the release of a protein from such gels cannot be modelled with a single value for the diffusion coefficient of the protein in the heterogeneous hydrogel matrix.

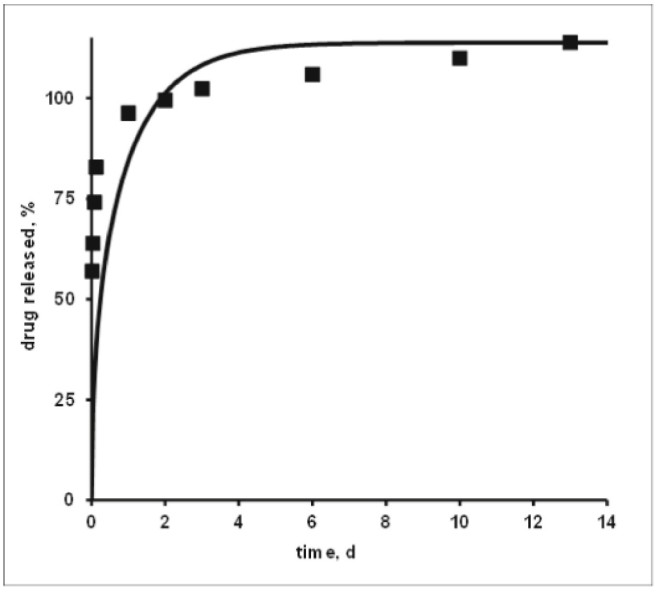

Fig. 6. FAB release from a hydrogel based on 5 wt% polymer. The curve shows the fitting of Eq. 1 to the experimental results (symbols). For Eq. 1, the experimentally determined plateau value was considered as M_∞.

3.3.2. *The structural integrity of the FAB protein during formulation and after release*

Fig. 7A shows the coomassie blue SDS-PAGE stains (under non-reducing conditions) of FAB incubated with PNF and PNM, at 4 °C (below LCST) and 37 °C (above LCST) for 3 h and 13 days. The hydrophilic non-thermosensitive 4 arm PEG-Mal was used as a positive control because this polymer has been previously shown to form protein-polymer conjugates [74,75] due to reaction of the maleimide functionality with SH and NH_2 groups of proteins. SDS-page analysis confirmed that PEG-Mal indeed reacted with FAB already after 3 h incubation in PBS at both 4 and 37 °C, and this reaction became more apparent after 13 days (as shown by the arrows in Fig. 7 A, likely pointing to the formation of PEG adducts with two FAB molecules). Fig. 7A also shows that PNF did not react with the FAB protein upon incubation for 3 h and 13 days at both 4 and 37 °C. However, FAB incubated with PNM for 13 days 4 °C showed a smear at higher apparent molecular weight of ~80–140

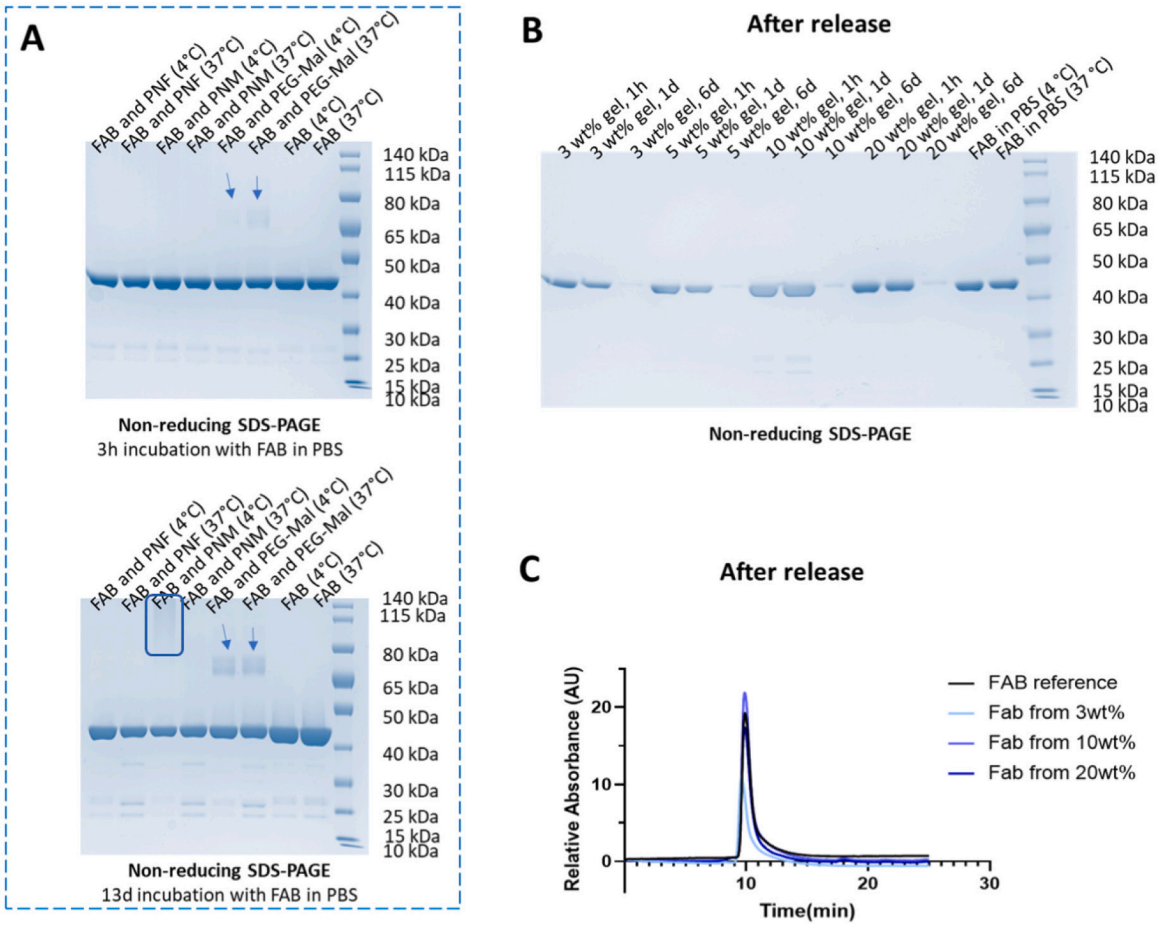

Fig. 7. Coomassie blue SDS-PAGE stains under non-reducing conditions of FAB incubated with PNF, PNM, and 4 arm PEG-Mal at 4 and 37 °C for 3 h and 13 days. B) Coomassie blue SDS-PAGE stains under non-reducing conditions of FAB released from 3, 5, 10, and 20 wt% PNF-PNM hydrogels after 1 h, 1 day, and 6 days. C) SEC-chromatogram of FAB released from 3, 10, and 20 wt% PNF-PNM hydrogels after 2 days. (For interpretation of the references to colour in this figure legend, the reader is referred to the web version of this article.)

kDa pointing to reaction of the maleimide groups of this polymer with the protein. Interestingly, the FAB protein did not react with PNM upon incubation at 37 °C for 13 days, likely because these groups are hidden in the hydrophobic domains of the gel formed above the LCST and were therefore not accessible for reaction with the protein. Importantly, SDS-page and SEC analysis of the released Fab did also not show modification of the protein (Fig. 7B, C) likely because the maleimide groups are present in the hydrophobic domains of the gels, and, moreover their concentration drops in time due to reaction with the furan groups during hydrogel chemical crosslinking by Diels Alder reaction.

3.3.3. *Release of dexamethasone from PNF-PNM hydrogels*

Fig. 8 shows the release profiles of dexamethasone from PNM-PNF hydrogels with different initial polymer content and the dissolution profile of dexamethasone crystals in PBS/tween. It is shown that the drug particles quantitatively dissolved within 5 days with ~90 % within the first day (Fig. 8A). On the other hand the same figure shows that after a small burst (~5% of the loading) sustained and almost quantitative release (around 95 % of the loaded amount) was observed in ~35 days which demonstrate the contribution of the hydrogel in prolonging the release of dexamethasone. Fig. 8 also shows that the different gels released their content with the same kinetics. It should be remarked that the gels have different cylindrical dimensions, and this thus points to a different diffusivity of the drug in the gel matrices. Given the low aqueous solubility (0.089 mg/mL) and log P (1.83) of dexamethasone [76], this drug is likely solubilized in the hydrophobic pNIPAM domains of the hydrogel. This design strategy allows for efficient loading and uniform distribution of dexamethasone within the hydrogel matrix. The obtained results suggest that the weight fraction of these domains of the hydrogel with the lowest initial polymer concentration (3 wt% gel) is already sufficient to dissolve the loaded dexamethasone dose. Indeed, the weight fraction of the hydrophobic domains is ~3 times higher than that of the drug.

Eq. 1 was fitted to the experimentally obtained release profiles. Fig. 9A shows an example for such a fitting. As it can be seen, the experimental data are well fitted with eq. 1. This was also true for the other investigated dexamethasone-loaded hydrogels, irrespective of the polymer concentration (Fig. 9B). The following apparent diffusion coefficients of dexamethasone in the investigated hydrogel matrices were calculated: $D = (13.0 \pm 0.4) \times 10^{-9}$, $(3.1 \pm 0.1) \times 10^{-9}$, and $(1.5 \pm 0.6) \times 10^{-9}$ cm^2/s for hydrogels based on 3, 10 and 20 % polymer, respectively (mean values +/− standard deviations, $n = 3$). These diffusion coefficients are, as expected, substantially smaller than the reported value in water (6800×10^{-9} cm^2/s [77]). Eq. 1 is derived under the assumption that the hydrogel structure is homogeneous, e.g. the existence of more hydrophobic vs. more hydrophilic regions with different drug mobilities is not considered. Thus, apparent diffusion coefficients are calculated, reflecting the overall dexamethasone mobility in the heterogenous hydrogel matrices. The observation that the determined apparent dexamethasone diffusion coefficient in the hydrogel decreases with increasing polymer concentration might be explained by the increasing volume fractions of hydrophobic pNIPAM domains in the hydrogel matrices, with lower drug mobility.

Using the mean values of the determined apparent dexamethasone

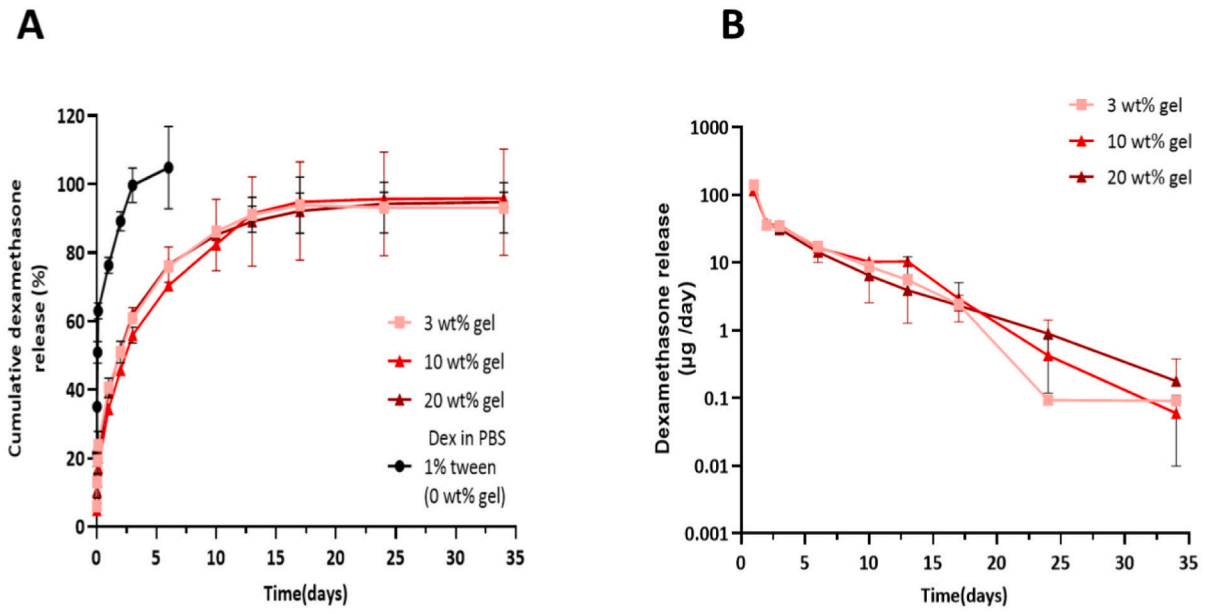

Fig. 8. A) Cumulative release profiles of dexamethasone (Dex) loaded PNF-PNM hydrogels in PBS 1 % tween at 37 °C with initial polymer concentrations of 3, 10 and 20 wt% of cylinders with diameters of 3.9, 2.3, 1.4 mm and of heights 4.3, 2.6, 1.6 mm, respectively, after hydrogel formation and water expulsion. These values are based weight measurement after hydrogel preparation assuming isotropic deswelling. Also shown is the dissolution of dexamethasone crystals dispersed in the release buffer. B) Dexamethasone released (in µg/day) from 3, 10, and 20 wt% PNF-PNM hydrogels.

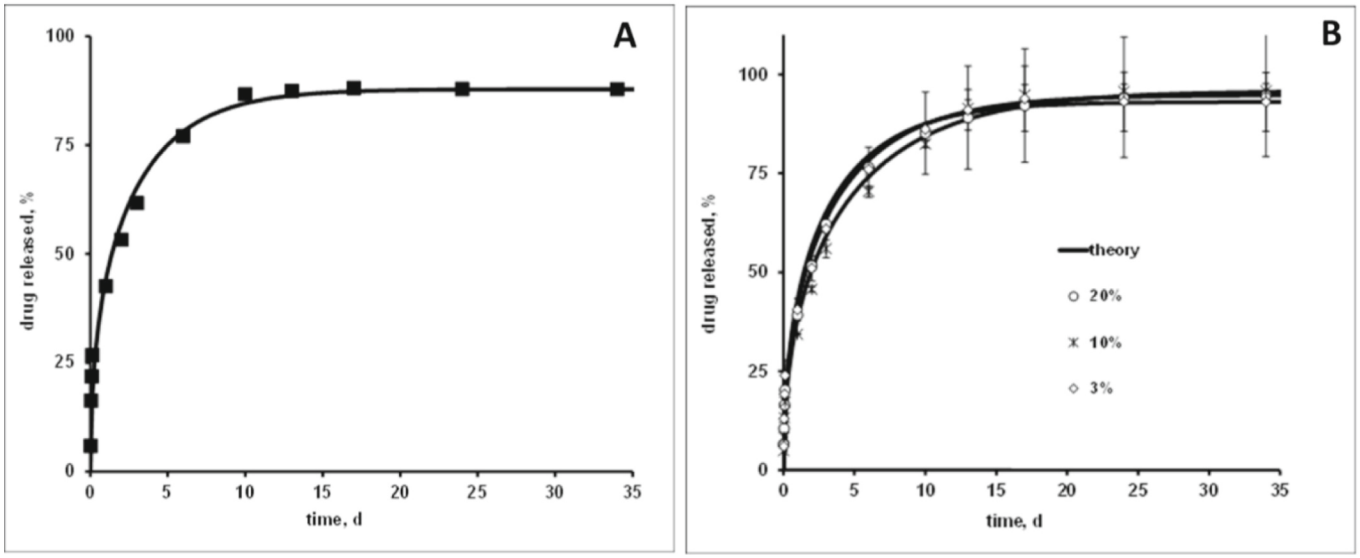

Fig. 9. A) Release of dexamethasone from a hydrogel based on 3 wt% polymer. The curve shows the fitting of Eq. 1 to the experimental results (symbols). B) the overall dexamethasone release from hydrogels based on 3, 10 or 20 wt% polymer (as indicated in the legend). For the experimental data points, mean values ± standard deviations (n = 3) are indicated.

diffusion coefficients, the drug release kinetics from different hydrogels were calculated and compared to the experimentally measured results. Fig. 9B shows the respective fitted and experimental data. The excellent agreement between Eq. 1 and the experimentally determined dexamethasone release kinetics suggests that the diffusion of the drug molecules through the hydrogel is much slower than the other phenomena and is thus the releasing-determining factor. For instance, dexamethasone partitioning between the more hydrophobic and more hydrophilic gel regions might is likely more rapid than drug diffusion through these regions.

Fig. 8B shows that the average amount of dexamethasone released per day for the gel formulations gradually decreased from ~100 to 0.1 µg/day over 35 days. The vitreous concentration of dexamethasone in patients that received 400 µg bolus injection of the drug was 25 ng/mL 3 days after intravitreal injection, with a half-life of 5.5h[12]. The only currently clinically available sustained release formulation for intraocular dexamethasone delivery is the OzurdexTM implant. This intravitreal implant results between 90 and 180 days in a concentration of 1.31 ± 1.94 pg/mL which still improves visual acuity [78]. In clinical use, the maximum volume for intravitreal injection in humans is 100 µL [79]. Therefore, the release rate of dexamethasone from the PNF-PNM hydrogel is expected to be sufficient for reaching the therapeutic range both in vitreous and retina for more 35 days after administration. As mentioned, the PNF-PNM hydrogel formulations demonstrated

controlled release of dexamethasone over a period of 35 days, with release rates ranging from 100 to 0.1 μg/day. This resulted in vitreous concentrations ranging from 25 to 0.025 μg/mL, considering the approximate vitreous volume of 4 mL. These concentrations are far above the therapeutic effective concentration based on clinical experience with the Ozurdex™ implant. It is worth noting that these concentrations still fall within the safe range observed in clinical practice. Fonseca et al. [80] conducted a clinical study showing that intravitreal administration of a 0.05 mL (200 μg) dexamethasone solution, with a concentration of 4 mg/mL, was safe and effectively reduced macular thickness secondary to diabetic macular edema (DME).

3.4. Cytocompatibility of PNF, PNM and PNF-PNM hydrogels

3.4.1. Cytotoxicity of RAW 264.7 and ARPE-19 cells exposed to PNF and PNM

The Alamar-Blue assay was conducted on RAW 264.7 and ARPE-19 cells, representing inflammatory cells macrophages and human retina cells, respectively, to determine the cell viability through the cells' metabolic activity. As shown in SI-fig. 6, unexpectedly, upon exposure of PNF to the cells, both RAW 264.7 and ARPE-19 cells showed metabolic activities over 100% compared to the control. The highest metabolic activities (153 ± 6% for RAW 264.7 cells and 169 ± 16% for ARPE-19 cells) were observed for the cells incubated with solutions of the highest PNF concentration (5 mg/mL). As a control, polymers were incubated in culture medium without cells for 24 h at 37 °C, whereafter the AlamarBlue assay was conducted. It was found that the polymers did not interfere with the assay. Seong et al. [81] reported that cell receptors can interact with hydrophobic portions (hyppos) of molecules. To prevent damage due these hyppos, cells activate repair and remodel pathways causing an increase in metabolic activity. Therefore, the observation of the higher metabolic activity of cells incubated with PNF might be ascribed to the hydrophobic character of the polymer at 37 °C. In contrast, reduced metabolic activities were found for RAW 264.7 and ARPE-19 cells when incubated with solutions of increasing PNM concentrations. Metabolic activities of cells incubated with solutions ≤1 mg/mL PNM were comparable with the positive control (cells incubated with medium only), while incubation of the cells with >1 mg/mL the solutions resulted in lower metabolic activities suggesting cytotoxicity. This higher toxicity for PNM as compared to PNF, is likely caused by the maleimide groups present, which might interact with membrane proteins resulting in a decrease in metabolic activity of the cells.

The cell cytocompatibility of PNF and PNM was also performed using a live-dead staining on RAW 264.7 and ARPE-19 cells (SI-fig. 8 and 9). In line with the results of the AlamarBlue assay, after 24 h of incubation at the studied concentrations (up to 5 mg/mL), PNF showed no toxicity to the RAW macrophages (Fig. 8A and B). In contrast, viability was compromised for RAW macrophages incubated with PNM in a concentration-dependent manner (Fig. 8A and B). Macrophages incubated with PNM (3–5 mg/mL) stained positive for both calcein and PI, showing that moribund cells still had active esterases present in the cytosol. The cells incubated with PNM at concentrations ≤1 mg/mL retained their viability which is in line with the results of the Alamar-Blue assay.

The results of the life-dead staining on the ARPE-19 cells retinal cells incubated with PNF and PNM at the same concentrations exhibited the same trend as observed for the macrophages (SI Fig. 9). ARPE-19 cells and RAW 264.7 cells showed comparable amounts of living cells after 24 h incubation with PNF (SI Fig. 9 A, B). The retina ARPE-19 cells incubated with solutions ≥2 mg/mL PNM stained majorly red, whereas the viability of cells incubated with PNM at concentration ≤ 1 mg/mL was not compromised.

Overall, it can be concluded form both assays that PNM showed no toxic effects. However, incubation of the cells with PNM caused toxic effects at concentrations >1 mg/mL. Noteworthy, for the aimed application the two complementary polymers are not administered separately, but are applied as an injectable formulation of the two polymers and thus cells are only exposed for a short time to the individual polymers as after injection of the formulation the temperature of the gel will increase to 37 °C (thus above the LCST) and physically and chemically crosslinked hydrogels will be formed.

To investigate whether the PNF-PNM system can be safely used as intraocular drug delivery system, human retina cells were cultured in direct contact with a PNF-PNM hydrogel for 24 h. Fig. 10 shows the ARPE- 19 cells proliferated in close contact with the gel and the cell viability was not affected by the hydrogel, showing the cytocompatibility of the PNF-PNM gel (SI-Fig. 7A, B).

4. Video: Intravitreal injection of PNF-PNM hydrogel through a 30 G needle into the vitreous body of an ex vivo rabbit eye

Injectability and syringeability are crucial for successful intravitreal drug delivery. Injectability ensures easy drug administration via a syringe, while syringeability refers to smooth drug withdrawal into the syringe. Optimizing these aspects enhances translational potential, benefiting treatment. In this study, a 10 wt% PNF-PNM hydrogel formulation was easily withdrawn and injected into the vitreous body of an ex vivo New Zealand rabbit eye. For more information and visual demonstration, the reader is referred to video 1 showing:

- Injection of 50 μL PNF-PNM formulation through a 30 G needle.
- After injection, followed by incubation of the eyeball at 37 °C for 3 h (to allow full chemical DA crosslinking), an incision was made to open the vitreous body.
- The hydrogel was visualized as white mass after the incision with a clear distinction from the transparent vitreous.

The results demonstrate that PNF-PNM formulation can be easily injected through a small 30G needle clinically recommended for intravitreal injections [82]. Furthermore, the PNF-PNM formulation crosslinked in situ the vitreous body by physical and subsequent chemical reactions and demonstrated its potential as a local drug delivery system for intraocular therapy. The hydrogel used in this study was intentionally designed to form a localized depot at the injection site. This particular characteristic of the hydrogel prevents it from dispersing throughout the vitreous humor, as it remains confined to a specific position. By localizing the hydrogel depot away from the visual pathway, potential disruptions to vision are minimized, as the hydrogel is not transparent, similar to many intraocular implants.

5. Conclusions

In this study, thermo-gelation was successfully combined with Diels Alder chemical crosslinking to design stable in situ forming hydrogels. This hydrogel is a versatile drug delivery system able to release two loaded drugs with different physicochemical properties (dexamethasone and FAB antibody fragment). The system can provide sustained release of dexamethasone for 35 days, while the FAB protein was released for 13 days. Interestingly, the maleimide functional group present in the hydrophobic domains of the polymer as well as in the formed hydrogel did not react with the protein at temperatures above LCST, avoiding unwanted protein modification during loading and release. The hydrogel is injectable through a 30 G needle and is well tolerated by retinal cells making the developed system a potential candidate for intravitreal drug therapy. In future directions, further preclinical and clinical investigations are necessary to determine the optimal dosing regimen and fully understand the impact of our hydrogel system on administration frequency. Additionally, exploring the applicability of our hydrogel system beyond ocular therapies, considering its sustained release capabilities, may uncover opportunities for in situ drug delivery in other applications.

Supplementary data to this article can be found online at https://doi.

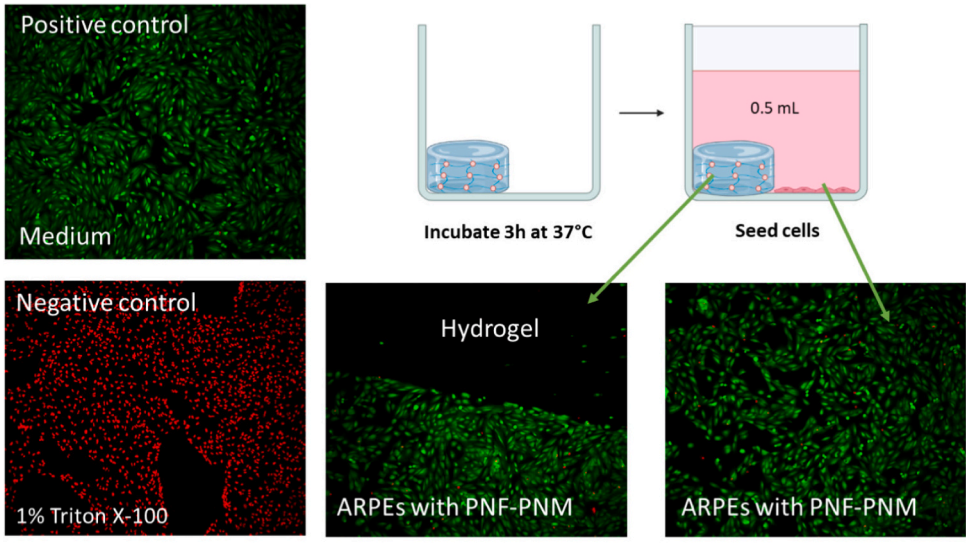

Fig. 10. Calcein AM and propidium iodide stainings of ARPE-19 cells cultured in the presence of a 10 wt% PNF-PNM hydrogel. Living cells are imaged green, and dying/dead cells are red. (For interpretation of the references to colour in this figure legend, the reader is referred to the web version of this article.)

org/10.1016/j.jconrel.2023.07.052.

CRediT authorship contribution statement

Blessing C. Ilochonwu: Conceptualization, Data curation, Investigation, Validation, Writing – original draft, Methodology. **Simone A. van der Lugt:** Investigation. **Ada Annala:** Investigation. **Greta Di Marco:** Investigation. **Thibault Sampon:** Investigation. **Juergen Siepmann:** Formal analysis, Writing – review & editing. **Florence Siepmann:** Formal analysis. **Wim E. Hennink:** Funding acquisition, Writing – review & editing. **Tina Vermonden:** Conceptualization, Funding acquisition, Project administration, Supervision, Writing – review & editing.

Declaration of Competing Interest

None.

Data availability

Data will be made available on request.

Acknowledgements

We thank Annemijn de Kleer for her contribution to this project. We also thank Dr. Achim Sauer for his kind advice and Boehringer Ingelheim for supplying the FAB antibody used in this study. This research was supported by funding from the European Union's Horizon 2020 research and innovation programme under the Marie Skłodowska-Curie grant agreement No 722717.

References

[1] R. Lee, T.Y. Wong, C. Sabanayagam, Epidemiology of diabetic retinopathy, diabetic macular edema and related vision loss, Eye Vis. (Lond) 2 (2015) 17.
[2] F.C. Gundogan, U. Yolcu, F. Akay, A. Ilhan, G. Ozge, S. Uzun, Diabetic macular edema, Pak. J. Med. Sci. 32 (2) (2016) 505–510.
[3] J.M. Colijn, G.H.S. Buitendijk, E. Prokofyeva, D. Alves, M.L. Cachulo, A. P. Khawaja, A. Cougnard-Gregoire, B.M.J. Merle, C. Korb, M.G. Erke, A. Bron, E. Anastasopoulos, M.A. Meester-Smoor, T. Segato, S. Piermarocchi, P. de Jong, J. R. Vingerling, F. Topouzis, C. Creuzot-Garcher, G. Bertelsen, N. Pfeiffer, A. E. Fletcher, P.J. Foster, R. Silva, J.F. Korobelnik, C. Delcourt, C.C.W. Klaver, consortium, E.-R.; European Eye Epidemiology, c, Prevalence of age-related macular degeneration in Europe: the past and the future, Ophthalmology 124 (12) (2017) 1753–1763.
[4] N. Karia, Retinal vein occlusion: pathophysiology and treatment options, Clin. Ophthalmol. 4 (2010) 809–816.
[5] R.K. Maturi, A.R. Glassman, D. Liu, R.W. Beck, A.R. Bhavsar, N.M. Bressler, L. M. Jampol, M. Melia, O.S. Punjabi, H. Salehi-Had, J.K. Sun, Diabetic Retinopathy Clinical Research, N, Effect of adding dexamethasone to continued ranibizumab treatment in patients with persistent diabetic macular edema: a DRCR network phase 2 randomized clinical trial, JAMA Ophthalmol. 136 (1) (2018) 29–38.
[6] A.N. Yuti Chernajovsky, Therapeutic Antibodies. Berlin vol. 181, 2008.
[7] S.A. Gaballa, U.B. Kompella, O. Elgarhy, A.M. Alqahtani, B. Pierscionek, R. G. Alany, H. Abdelkader, Corticosteroids in ophthalmology: drug delivery innovations, pharmacology, clinical applications, and future perspectives, Drug Deliv. Transl. Res. 11 (3) (2021) 866–893.
[8] E. Donnenfeld, E. Holland, Dexamethasone intracameral drug-delivery suspension for inflammation associated with cataract surgery: a randomized, placebo-controlled, Phase III Trial, Ophthalmology 125 (6) (2018) 799–806.
[9] N.V. Saraiya, D.A. Goldstein, Dexamethasone for ocular inflammation, Expert. Opin. Pharmacother. 12 (7) (2011) 1127–1131.
[10] A. Farkouh, P. Frigo, M. Czejka, Systemic side effects of eye drops: a pharmacokinetic perspective, Clin. Ophthalmol. 10 (2016) 2433–2441.
[11] C.H. Meyer, T.U. Krohne, P. Charbel Issa, Z. Liu, F.G. Holz, Routes for drug delivery to the eye and retina: intravitreal injections, Dev. Ophthalmol. 55 (2016) 63–70.
[12] I.M. Gan, L.C. Ugahary, J.T. van Dissel, J.C. van Meurs, Effect of intravitreal dexamethasone on vitreous vancomycin concentrations in patients with suspected postoperative bacterial endophthalmitis, Graefes Arch. Clin. Exp. Ophthalmol. 243 (11) (2005) 1186–1189.
[13] S.J. Bakri, M.R. Snyder, J.M. Reid, J.S. Pulido, M.K. Ezzat, R.J. Singh, Pharmacokinetics of intravitreal ranibizumab (Lucentis), Ophthalmology 114 (12) (2007) 2179–2182.
[14] K. Radhakrishnan, N. Sonali, M. Moreno, J. Nirmal, A.A. Fernandez, S. Venkatraman, R. Agrawal, Protein delivery to the back of the eye: barriers, carriers and stability of anti-VEGF proteins, Drug Discov. Today 22 (2) (2017) 416–423.
[15] E.M. Del Amo, A.K. Rimpela, E. Heikkinen, O.K. Kari, E. Ramsay, T. Lajunen, M. Schmitt, L. Pelkonen, M. Bhattacharya, D. Richardson, A. Subrizi, T. Turunen, M. Reinisalo, J. Itkonen, E. Toropainen, M. Casteleijn, H. Kidron, M. Antopolsky, K. S. Vellonen, M. Ruponen, A. Urtti, Pharmacokinetic aspects of retinal drug delivery, Prog. Retin. Eye Res. 57 (2017) 134–185.
[16] A. Patel, K. Cholkar, V. Agrahari, A.K. Mitra, Ocular drug delivery systems: an overview, World J. Pharmacol. 2 (2) (2013) 47–64.
[17] A. Mandal, R. Bisht, I.D. Rupenthal, A.K. Mitra, Polymeric micelles for ocular drug delivery: from structural frameworks to recent preclinical studies, J. Control. Release 248 (2017) 96–116.
[18] P. Bansal, S. Garg, Y. Sharma, P. Venkatesh, Posterior segment drug delivery devices: current and novel therapies in development, J. Ocul. Pharmacol. Ther. 32 (3) (2016) 135–144.
[19] L.L. Lim, J.R. Smith, J.T. Rosenbaum, Retisert (Bausch & Lomb/control delivery systems), Curr. Opin. Investig. Drugs 6 (11) (2005) 1159–1167.
[20] G.J. Jaffe, D. Martin, D. Callanan, P.A. Pearson, B. Levy, T. Comstock, Fluocinolone Acetonide Uveitis Study, G, Fluocinolone acetonide implant (Retisert) for noninfectious posterior uveitis: thirty-four-week results of a multicenter randomized clinical study, Ophthalmology 113 (6) (2006) 1020–1027.
[21] F.E. Kane, J. Burdan, A. Cutino, K.E. Green, Iluvien: a new sustained delivery technology for posterior eye disease, Exp. Opin. Drug. Deliv. 5 (9) (2008) 1039–1046.

[22] D.S. Boyer, Y.H. Yoon, R. Belfort Jr., F. Bandello, R.K. Maturi, A.J. Augustin, X. Y. Li, H. Cui, Y. Hashad, S.M. Whitcup, M.S.G. Ozurdex, Three-year, randomized, sham-controlled trial of dexamethasone intravitreal implant in patients with diabetic macular edema, Ophthalmology 121 (10) (2014) 1904–1914.

[23] A. Chan, L.S. Leung, M.S. Blumenkranz, Critical appraisal of the clinical utility of the dexamethasone intravitreal implant (Ozurdex) for the treatment of macular edema related to branch retinal vein occlusion or central retinal vein occlusion, Clin. Ophthalmol. 5 (2011) 1043–1049.

[24] J. Wang, A. Jiang, M. Joshi, J. Christoforidis, Drug delivery implants in the treatment of vitreous inflammation, Mediat. Inflamm. 2013 (2013), 780634.

[25] ClinicalTrials.gov, Extension Study for the Port Delivery System With Ranibizumab (Portal) (Portal), https://clinicaltrials.gov/ct2/show/NCT03683251 (accessed May 22, 2021), 2018.

[26] ClinicalTrials.gov, Study of the Efficacy and Safety of the Ranibizumab Port Delivery System (RPDS) for Sustained Delivery of Ranibizumab in Participants with Subfoveal Neovascular Age-Related Macular Degeneration (AMD) (LADDER), https://clinicaltrials.gov/ct2/show/NCT02510794 (accessed May 05, 2021), 2015.

[27] ClinicalTrials.gov, A Phase III Study to Evaluate the Port Delivery System With Ranibizumab Compared With Monthly Ranibizumab Injections in Participants With Wet Age-Related Macular Degeneration (Archway), https://clinicaltrials.gov/ct2/show/NCT03677934?term=archway&rank=1 (accessed May 22, 2021), 2021.

[28] M.J. Ansari, R.R. Rajendran, S. Mohanto, U. Agarwal, K. Panda, K. Dhotre, R. Manne, A. Deepak, A. Zafar, M. Yasir, S. Pramanik, Poly(N-isopropylacrylamide)-based hydrogels for biomedical applications: a review of the state-of-the-art, Gels 8 (7) (2022) 454.

[29] T. Vermonden, R. Censi, W.E. Hennink, Hydrogels for protein delivery, Chem. Rev. 112 (5) (2012) 2853–2888.

[30] Y. Li, H.Y. Yang, D.S. Lee, Biodegradable and injectable hydrogels in biomedical applications, Biomacromolecules 23 (3) (2022) 609–618.

[31] B.C. Ilochonwu, A. Urtti, W.E. Hennink, T. Vermonden, Intravitreal hydrogels for sustained release of therapeutic proteins, J. Control. Release 326 (2020) 419–441.

[32] D. Chang, K. Park, A. Famili, Hydrogels for sustained delivery of biologics to the back of the eye, Drug Discov. Today 24 (8) (2019) 1470–1482.

[33] J. Li, D.J. Mooney, Designing hydrogels for controlled drug delivery, Nat. Rev. Mater. 1 (12) (2016) 1–17.

[34] S.R. Van Tomme, W.E. Hennink, Biodegradable dextran hydrogels for protein delivery applications, Exp. Rev. Med. Dev. 4 (2) (2007) 147–164.

[35] S. Kirchhof, A. Strasser, H.-J. Wittmann, V. Messmann, N. Hammer, A. M. Goepferich, F.P. Brandl, New insights into the cross-linking and degradation mechanism of Diels–Alder hydrogels, J. Mater. Chem. B 3 (3) (2015) 449–457.

[36] H. Shah, E. Reichel, B. Busbee, A novel lidocaine hydrochloride ophthalmic gel for topical ocular anesthesia, Local Reg. Anesthesia 3 (2010) 57–63.

[37] I. Kozak, L. Cheng, W.R. Freeman, Lidocaine gel anesthesia for intravitreal drug administration, Retina 25 (8) (2005) 994–998.

[38] B.C. Ilochonwu, M. Mihajlovic, R.F. Maas-Bakker, C. Rousou, M. Tang, M. Chen, W. E. Hennink, T. Vermonden, Hyaluronic acid-PEG-based Diels-Alder in situ forming hydrogels for sustained intraocular delivery of bevacizumab, Biomacromolecules 23 (7) (2022) 2914–2929.

[39] S. Kirchhof, M. Gregoritza, V. Messmann, N. Hammer, A.M. Goepferich, F. P. Brandl, Diels-Alder hydrogels with enhanced stability: first step toward controlled release of bevacizumab, Eur. J. Pharm. Biopharm. 96 (2015) 217–225.

[40] Q. Chai, Y. Jiao, X. Yu, Hydrogels for biomedical applications: their characteristics and the mechanisms behind them, Gels 3 (1) (2017) 6.

[41] P. Sikdar, M.M. Uddin, T.M. Dip, S. Islam, M.S. Hoque, A.K. Dhar, S. Wu, Recent advances in the synthesis of smart hydrogels, Mater. Adv. 2 (14) (2021) 4532–4573.

[42] H.M. El-Husseiny, E.A. Mady, L. Hamabe, A. Abugomaa, K. Shimada, T. Yoshida, T. Tanaka, A. Yokoi, M. Elbadawy, R. Tanaka, Smart/stimuli-responsive hydrogels: cutting-edge platforms for tissue engineering and other biomedical applications, Mater. Today Bio. 13 (2022), 100186.

[43] X. Xu, J. Yu, H. Shi, J. Zhang, X. Li, Prevention of corneal neovascularization by subconjunctival injection of avastin(R) loaded thermosensitive hydrogels in rabbit model, Int. J. Pharm. 552 (1–2) (2018) 164–170.

[44] J.J.K. Derwent, W.F. Mieler, Thermoresponsive hydrogels as a new ocular drug delivery platform to the posterior segment of the eye, Trans. Am. Ophthalmol. Soc. 106 (2008) 206–214.

[45] M.A. Haq, Y. Su, D. Wang, Mechanical properties of PNIPAM based hydrogels: a review, Mater. Sci. Eng. C Mater. Biol. Appl. 70 (Pt 1) (2017) 842–855.

[46] A. Alexander, Ajazuddin, J. Khan, S. Saraf, S. Saraf, Polyethylene glycol (PEG)-Poly (N-isopropylacrylamide) (PNIPAAm) based thermosensitive injectable hydrogels for biomedical applications, Eur. J. Pharm. Biopharm. 88 (3) (2014) 575–585.

[47] V. Cheng, B.H. Lee, C. Pauken, B.L. Vernon, Poly(N-isopropylacrylamide-co-poly (ethylene glycol))-acrylate simultaneously physically and chemically gelling polymer systems, J. Appl. Polym. Sci. 106 (2) (2007) 1201–1207.

[48] O. Diels, K. Alder, Synthesen in der hydro-aromatischen Reihe, II. Mitteilung: Über Cantharidin, Berichte der deutschen chemischen Gesellschaft (A and B Series) 62 (3) (1929) 554–562.

[49] Hong-Liang Wei, Zhe Yang, Li-Mei Zheng, Y.-M. Shen, Thermosensitive hydrogels synthesized by fast Diels–Alder reaction in water, Polymer 50 (13) (2009) 2836–2840.

[50] C.M. Madl, S.C. Heilshorn, Bioorthogonal strategies for engineering extracellular matrices, Adv. Funct. Mater. 28 (11) (2018).

[51] A.J. de Graaf, K.W. Boere, J. Kemmink, R.G. Fokkink, C.F. van Nostrum, D. T. Rijkers, J. van der Gucht, H. Wienk, M. Baldus, E. Mastrobattista, T. Vermonden, W.E. Hennink, Looped structure of flowerlike micelles revealed by 1H NMR relaxometry and light scattering, Langmuir 27 (16) (2011) 9843–9848.

[52] J. Loccufier, M. Bos, E.H. Schacht, Convenient method for the analysis of primary and secondary hydroxyl end groups in polyethers, Polym. Bull. 27 (1991) 201–204.

[53] O. Soga, C.F. van Nostrum, A. Ramzi, T. Visser, F. Soulimani, P.M. Frederik, P.H. H. Bomans, W.E. Hennink, Physicochemical characterization of degradable thermosensitive polymeric micelles, Langmuir 20 (21) (2004) 9388–9395.

[54] P.J. Flory Jr., J. R, Statistical mechanics of cross-linked polymer networks I. rubberlike elasticity, J. Chem. Phys. 11 (11) (1943) 512–520.

[55] H.G. Schild, Poly(N-isopropylacrylamide): experiment, theory and application, Prog. Polym. Sci. 17 (2) (1992) 163–249.

[56] E.H. Marzieh Najafi, E. Wim, Tina Vermonden Hennink, Poly (Nisopropylacrylamide): Physicochemical Properties and Biomedical Applications, John Wiley Sons, Ltd, 2018.

[57] A. Durand, D. Hourdet, Thermoassociative graft copolymers based on poly(N-isopropylacrylamide): relation between the chemical structure and the rheological properties, Macromol. Chem. Phys. 201 (8) (2000) 858–868.

[58] R.G. Huber, M.A. Margreiter, J.E. Fuchs, S. von Grafenstein, C.S. Tautermann, K. R. Liedl, T. Fox, Heteroaromatic pi-stacking energy landscapes, J. Chem. Inf. Model. 54 (5) (2014) 1371–1379.

[59] F.R. Cordell, J.E. Boggs, Structure and degree of aromatic character in furan, pyrrole, and thiophene, J. Mol. Struct. THEOCHEM 85 (1) (1981) 163–178.

[60] L. Ahmadkhani, M. Abbasian, A. Akbarzadeh, Synthesis of sharply thermo and PH responsive PMA-b-PNIPAM-b-PEG-b-PNIPAM-b-PMA by RAFT radical polymerization and its schizophrenic micellization in aqueous solutions, Des Monomers Polym. 20 (1) (2017) 406–418.

[61] J. Yang, R. van Lith, K. Baler, R.A. Hoshi, G.A. Ameer, A thermoresponsive biodegradable polymer with intrinsic antioxidant properties, Biomacromolecules 15 (11) (2014) 3942–3952.

[62] R. Li, Y. Wu, Z. Bai, J. Guo, X. Chen, Effect of molecular weight of polyethylene glycol on crystallization behaviors, thermal properties and tensile performance of polylactic acid stereocomplexes, RSC Adv. 10 (69) (2020) 42120–42127.

[63] C.M. Nimmo, S.C. Owen, M.S. Shoichet, Diels-Alder click cross-linked hyaluronic acid hydrogels for tissue engineering, Biomacromolecules 12 (3) (2011) 824–830.

[64] O. El Tall, Y. Hou, E. Abou-Hamad, I.U. Raja, M.N. Hedhili, W. Peng, R. Mahfouz, O.M. Bakr, P.M. Beaujuge, Direct functionalization of Nanodiamonds with Maleimide, Chem. Mater. 26 (9) (2014) 2766–2769.

[65] T. Sepperer, J. Neubauer, J. Eckardt, T. Schnabel, A. Petutschnigg, G. Tondi, Pollutant absorption as a possible end-of-life solution for polyphenolic polymers, Polymers (Basel) 11 (5) (2019).

[66] G. Tondi, M. Link, C.W. Oo, A. Petutschnigg, A simple approach to distinguish classic and formaldehyde-free tannin based rigid foams by ATR FT-IR, J. Spectroscopy 2015 (2015) 1–8.

[67] A. Oluwasanmi, C. Hoskins, Potential use of the Diels-Alder reaction in biomedical and nanomedicine applications, Int. J. Pharm. 604 (2021), 120727.

[68] D. Neradovic, M.J. van Steenbergen, L. Vansteelant, Y.J. Meijer, C.F. van Nostrum, W.E. Hennink, Degradation mechanism and kinetics of thermosensitive polyacrylamides containing lactic acid side chains, Macromolecules 36 (20) (2003) 7491–7498.

[69] S. Aretz, T.U. Krohne, K. Kammerer, U. Warnken, A. Hotz-Wagenblatt, M. Bergmann, B.V. Stanzel, T. Kempf, F.G. Holz, M. Schnölzer, J. Kopitz, In-depth mass spectrometric mapping of the human vitreous proteome, Proteome Sci. 11 (1) (2013) 22.

[70] L.M. Hirvonen, G.O. Fruhwirth, N. Srikantha, M.J. Barber, J.E. Neffendorf, K. Suhling, T.L. Jackson, Hydrodynamic radii of ranibizumab, aflibercept and bevacizumab measured by time-resolved phosphorescence anisotropy, Pharm. Res. 33 (8) (2016) 2025–2032.

[71] R. Censi, T. Vermonden, H. Deschout, K. Braeckmans, P. di Martino, S.C. De Smedt, C.F. van Nostrum, W.E. Hennink, Photopolymerized thermosensitive poly (HPMAlactate)-PEG-based hydrogels: effect of network design on mechanical properties, degradation, and release behavior, Biomacromolecules 11 (8) (2010) 2143–2151.

[72] J. Crank, Diffuision in a plane sheet, in: The Mathematics of Diffusion, 1975, pp. 47–48.

[73] J. Siepmann, F. Siepmann, Modeling of diffusion controlled drug delivery, J. Control. Release 161 (2) (2012) 351–362.

[74] M.J. Roberts, M.D. Bentley, J.M. Harris, Chemistry for peptide and protein PEGylation, Adv. Drug Deliv. Rev. 54 (4) (2002) 459–476.

[75] N. Hammer, F.P. Brandl, S. Kirchhof, V. Messmann, A.M. Goepferich, Protein compatibility of selected cross-linking reactions for hydrogels, Macromol. Biosci. 15 (3) (2015) 405–413.

[76] online, D. Dexamethasone https://go.drugbank.com/drugs/DB01234 (accessed 13/07/2022).

[77] R. Schulz, K. Yamamoto, A. Klossek, R. Flesch, S. Honzke, F. Rancan, A. Vogt, U. Blume-Peytavi, S. Hedtrich, M. Schafer-Korting, E. Ruhl, R.R. Netz, Data-based modeling of drug penetration relates human skin barrier function to the interplay of diffusivity and free-energy profiles, Proc. Natl. Acad. Sci. U. S. A. 114 (14) (2017) 3631–3636.

[78] J.E. Chang-Lin, M. Attar, A.A. Acheampong, M.R. Robinson, S.M. Whitcup, B. D. Kuppermann, D. Welty, Pharmacokinetics and pharmacodynamics of a sustained-release dexamethasone intravitreal implant, Invest. Ophthalmol. Vis. Sci. 52 (1) (2011) 80–86.

[79] A. Grzybowski, R. Told, S. Sacu, F. Bandello, E. Moisseiev, A. Loewenstein, U. Schmidt-Erfurth, B. Euretina, 2018 update on intravitreal injections: Euretina expert consensus recommendations, Ophthalmologica 239 (4) (2018) 181–193.

[80] A.L.A. Fonseca, H. Panetta, M.A. Nascimento, R.P.C. Lira, C.E.L. Arieta, Effect of intravitreal dexamethasone solution on the reduction of macular thickness in

pseudophakic diabetic patients in a public hospital in Brazil: a randomized clinical trial, Clin. Ophthalmol. 13 (2019) 1523–1531.
[81] S.-Y. Seong, P. Matzinger, Hydrophobicity: an ancient damage-associated molecular pattern that initiates innate immune responses, Nat. Rev. Immunol. 4 (6) (2004) 469–478.
[82] R.R. Hartman, U.B. Kompella, Intravitreal, subretinal, and suprachoroidal injections: evolution of microneedles for drug delivery, J. Ocul. Pharmacol. Ther. 34 (1–2) (2018) 141–153.